Polytechnic Institute of New York

SUPPRESSION OF INTERCHANNEL INTERFERENCE IN FM RECEIVERS

FINAL TECHNICAL REPORT

Frank A. Cassara
Harry Schachter

JULY 1979

U.S. ARMY RESEARCH OFFICE

Grant No. DAAG 29-77-G-0232

Polytechnic Institute of New York

Report No. POLY EE 79-056

Approved for public release; Distribution Unlimited

UNCLASSIFIED

SECURITY CLASSIFICATION OF THIS PAGE (When Data Entered)

REPORT DOCUMENTATION PAGE	READ INSTRUCTIONS BEFORE COMPLETING FORM
1. REPORT NUMBER / 2. GOVT ACCESSION NO.	3. RECIPIENT'S CATALOG NUMBER
4. TITLE (and Subtitle) Suppression of Interchannel Interference in FM Receivers.	5. TYPE OF REPORT & PERIOD COVERED Final Technical Report 9/30/77 to 6/29/79
	6. PERFORMING ORG. REPORT NUMBER POLY-EE 79-056
7. AUTHOR(s) Frank A. Cassara Harry Schachter	8. CONTRACT OR GRANT NUMBER(s) Grant DAAG 29-77-G-0232
9. PERFORMING ORGANIZATION NAME AND ADDRESS Polytechnic Institute of New York, Department of Electrical Engineering Brooklyn, N. Y. 11201	10. PROGRAM ELEMENT, PROJECT, TASK AREA & WORK UNIT NUMBERS
11. CONTROLLING OFFICE NAME AND ADDRESS U. S. Army Research Office Post Office Box 12211 Research Triangle Park, N.C. 27709	12. REPORT DATE July 1979 13. NUMBER OF PAGES 66
14. MONITORING AGENCY NAME & ADDRESS (if different from Controlling Office)	15. SECURITY CLASS. (of this report) Unclassified 15a. DECLASSIFICATION/DOWNGRADING SCHEDULE

16. DISTRIBUTION STATEMENT (of this Report)

Approved for public release; distribution unlimited

17. DISTRIBUTION STATEMENT (of the abstract entered in Block 20, if different from Report)

18. SUPPLEMENTARY NOTES

The findings in this report are not to be construed as an official Department of the Army position, unless so designated by other authorized documents.

19. KEY WORDS (Continue on reverse side if necessary and identify by block number)

phase-locked loop
interchannel interference
frequency modulation

20. ABSTRACT (Continue on reverse side if necessary and identify by block number)

In this work an FM detector capable of suppressing the degradation in receiver performance due to the presence of an interfering signal is presented. Optimum receiver structures based on maximum-a-posteriori estimation procedures are first theoretically derived and then a practical demodulator based on the optimum receivers is examined. The receiver consists of two phase-locked loops (PLL) cross coupled in such a manner as to permit one PLL to lock on to and track the stronger received FM signal while the other loop tracks the weaker of

DD FORM 1 JAN 73 1473 EDITION OF 1 NOV 65 IS OBSOLETE

UNCLASSIFIED

SECURITY CLASSIFICATION OF THIS PAGE (When Data Entered)

20 (Abstract)

the two received FM signals. The detector has the capability of demodulating both the desired received FM as well as the interferer even for the case when both signals are co-channel. Experimental results demonstrating such capability even in the presence of strong input gaussian noise are presented along with a computer simulation study examining the transient acquisition behavior of the cross coupled PLL receiver structure.

TABLE OF CONTENTS

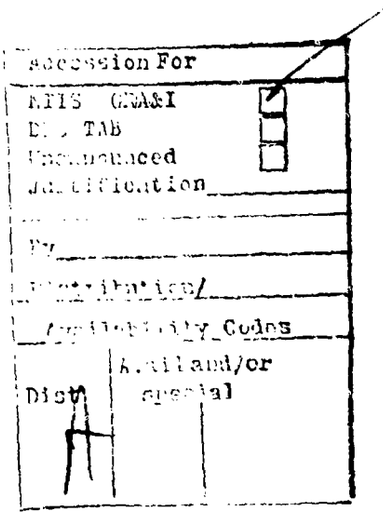

TABLE OF FIGURES

SUPPRESSION OF INTERCHANNEL INTERFERENCE IN FM RECEIVERS

Frank A. Cassara and Harry Schachter
Polytechnic Institute of New York
Route 110
Farmingdale, New York 11735

Abstract

In this work an FM detector capable of suppressing the degradation in receiver performance due to the presence of an interfering signal is presented. Optimum receiver structures based on maximum-a-posteriori estimation procedures are first theoretically derived and then a practical demodulator based on the optimum receivers is examined. The receiver consists of two phase-locked loops (PLL) cross coupled in such a manner as to permit one PLL to lock on to and track the stronger received FM signal while the other loop tracks the weaker of the two received FM signals. The detector has the capability of demodulating both the desired received FM as well as the interferer even for the case when both signals are co-channel. Experimental results demonstrating such capability even in the presence of strong input gaussian noise are presented along with a computer simulation study examining the transient acquisition behavior of the cross coupled PLL receiver structure.

to noise ratio of 12dB to less than 10^{-5} at the same ratio when the carrier strength of the echo is only 30% of the dominant path signal. Similar degradations were experimentally obtained by Gutwein and Bland [5] as well as Salven and Duncombe [6]. Panter [7] has shown how FM multipath phase errors in an analog FM system can lead to significant errors in range measurements.

Interfering signals can arise in the following general areas:

1. Co-channel Interferer:

(a) neighboring transmitters sharing the same frequency band. An example of this is the mutual interference that exists between communication satellites and terrestrial microwave communication links.

(b) spurious signals such as an image channel in a superheterodyne receiver.

(c) multipath echoes resulting from reflections off buildings or other obstructions.

2. Adjacent Channel Interferer:

(a) inadequate selectivity in the receiver's IF filter.

(b) "crowding" in the radio frequency spectrum.

(c) spurious signals.

To date the most popular technique in suppressing interferers has been steerable antenna null techniques. Such arrays establish spatial nulls in the direction of the interferer(s) and have been successful in suppressing a variety of interferers. However, steerable antenna null techniques have experienced a number of problems. Among these include:

(1) when the source of interference comes from the same direction as the desired signal both the interferer and desired signal are nulled.

(2) when the interferer to desired signal carrier amplitude ratio approaches unity the performance of the system degrades severely.

(3) military personnel have opposed the use of multiple antenna elements in some applications.

(4) acquisition time for the antenna array to attack the jammer can be rather long for some algorithms.

(5) wide bandwidth nulls have been difficult to obtain.

In this paper a novel FM detector which has demonstrated capability in suppressing the degradation in receiver performance due to the presence of an interfering signal and not experience the difficulties enumerated for the steerable antenna null techniques is presented. First the evolution of the detector structure through maximum-a-posteriori (MAP) estimation procedures is demonstrated; an optimum (though unrealizable) receiver structure is derived. Then, experimental results on a detector designed by copying the topology of the optimum receiver structure are presented along with a computer simulation study examining the transient acquisition behavior of the cross coupled PLL receiver structure.

II. Maximum-A-Posteriori Optimum Receiver

Consider a received FM signal with the interchannel interference and additive gaussian noise which may be represented mathematically as

$$v(t) = s_1(t) + s_2(t) + n(t) , \quad o \leq t \leq T \tag{1}$$

where

$$s_1(t) = A_1 \cos \left(\omega_1 t + \int^t m_1(u)\, du\right)$$

$$s_2(t) = A_2 \cos \left(\omega_2 t + \int^t m_2(u)\, du\right)$$

$n(t)$ is white gaussian noise with zero mean and normalized two sided power spectral density of 1 watt/Hz.

$m_1(t)$ is the desired signal modulation

$m_2(t)$ is the modulation on the interfering FM wave.

A_1 and A_2 are assumed constant

$m_1(t)$ and $m_2(t)$ are assumed to be independent stationary gaussian processes with zero mean and autocorrelation $R_{m_1}(\tau)$ and $R_{m_2}(\tau)$.

We designate

$$x_1(t) = \int^t m_1(u)\, du \tag{2}$$

$$x_2(t) = \int^t m_2(u)\, du \tag{3}$$

This converts the FM waves $s_1(t)$ and $s_2(t)$ into angle modulated waves with $x_1(t)$ and $x_2(t)$ as modulating signals. It is seen that $x_1(t)$ and $x_2(t)$

are also mutually independent zero mean gaussian random processes. Let the autocorrelation functions of $x_1(t)$ and $x_2(t)$ be denoted by $R_{x_1}(\tau)$ and $R_{x_2}(\tau)$.

We now derive a MAP receiver for the optimum reception of $m_1(t)$. Van trees[8] has proved that a linear operation on the MAP estimate of a continuous random process is equal to the MAP estimate of the output of the linear operation performed on the random process. Therefore MAP estimation of $x_1(t)$ and subsequent differentiation of the estimate $\hat{x}_1(t)$ will give the MAP estimate $\hat{m}_1(t)$ of $m_1(t)$. We follow this procedure. We use abstract vector space methods throughout as developed by Schwartz[9]. We do not indicate the time-dependence of variables in the interest of brevity unless where explicitly necessary.

The controlling relation for MAP estimation of $x_1(t)$ is[9]

$$\frac{\partial p(x_1|v)}{\partial x_1} = 0 \tag{4}$$

where $p(x_1|v)$ is the conditional probability density function of x_1 given the received signal $v(t)$. Eq. (4) can be written in the following equivalent form

$$\frac{\partial}{\partial x_1} \log p(x_1|v) = 0 \tag{5}$$

Using the relation

$$p(x_1|v) = p(v|x_1) \cdot p(x_1)/p(v)$$

and

$$\frac{\partial p(v)}{\partial x_1} = 0$$

we obtain

$$\frac{\partial}{\partial x_1} \text{og } p(v/x_1) + \frac{\partial}{\partial x_1} \log p(x_1) = 0 \tag{6}$$

The evaluation of the two parts of Eq. (6) are given in Appendix A. The solution of Eq. (6) for $x_1(t)$ is the MAP estimate which we denote by $\hat{x}_1(t)$ and as shown in Appendix A is given by

$$\hat{x}_1(t) = k_1 \int_o^T R_{x_1}(t, u) \frac{\partial \hat{s}_1}{\partial x_1} (v - \bar{s}_2) du \tag{7}$$

where k_1 denotes a constant, $R_{x_1}(t, u)$ is the impulse response of a low pass filter, and $\bar{s}_2$ represents the minimum mean square estimate of $s_2(t)$.

According to Eq. (7) the MAP estimate $\hat{x}_1(t)$ can be obtained from the phase-locked loop structure shown in Fig. 1 with $\overline{s_2(t)}$ as an external input.

In a similar manner estimating $x_2(t)$ instead of $x_1(t)$ we obtain

$$\hat{x}_2(t) = k_2 \int_o^T R_{x_2}(t, u) \frac{\partial \hat{s}_2}{\partial x_2} \cdot (v - \bar{s}_1) du \tag{8}$$

This is a receiver identical to Fig. 1 except that $\bar{s}_2$ is replaced by $\bar{s}_1$ and $R_{x_1}(t, \mu)$ is replaced by $R_{x_2}(t, u)$. If we assume $\bar{s}_1$ and $\bar{s}_2$ are suitable estimates of $\hat{s}_1$ and $\hat{s}_2$, respectively, i. e., the m. m. s. e. are approximately equal to the MAP estimates, then the receiver of Fig. 1 and its equivalent for obtaining $\hat{x}_2(t)$ can be coupled to obtain a comprehensive receiver with no unknown inputs. Recalling that in the case of FM, the modulation functions are $m_1(t) = \dot{x}_1(t)$ and $m_2(t) = \dot{x}_2(t)$ and replacing the phase controlled voltage controlled oscillator (VCO) of Fig. 1 by a frequency controlled VCO, such a cross coupled FM receiver appears as in Fig. 2. It must be emphasized that only when $\hat{s}_1(t) = \bar{s}_1(t)$ and $\hat{s}_2(t) = \bar{s}_2(t)$ will this receiver be optimum.

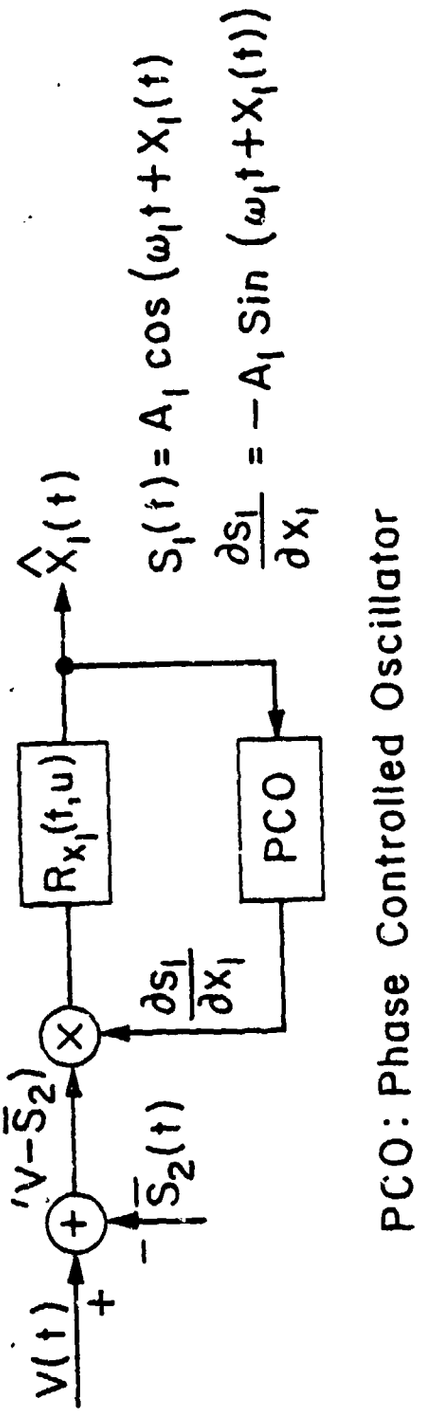

Fig. 1 Optimum Receiver for $x_1(t)$

$$\frac{\partial \hat{s}_1}{\partial x_1} = -A_1 \sin\left(\omega_1 t + \int^t \hat{m}_1(u)\,du\right)$$

$$h_1(t,t') = \int^{t'} R_{m_1}(t,u)\,du$$

$$\frac{\partial \hat{s}_2}{\partial x_2} = -A_2 \sin\left(\omega_2 t + \int^t \hat{m}_2(u)\,du\right)$$

$$h_2(t,t') = \int^{t'} R_{m_2}(t,u)\,du$$

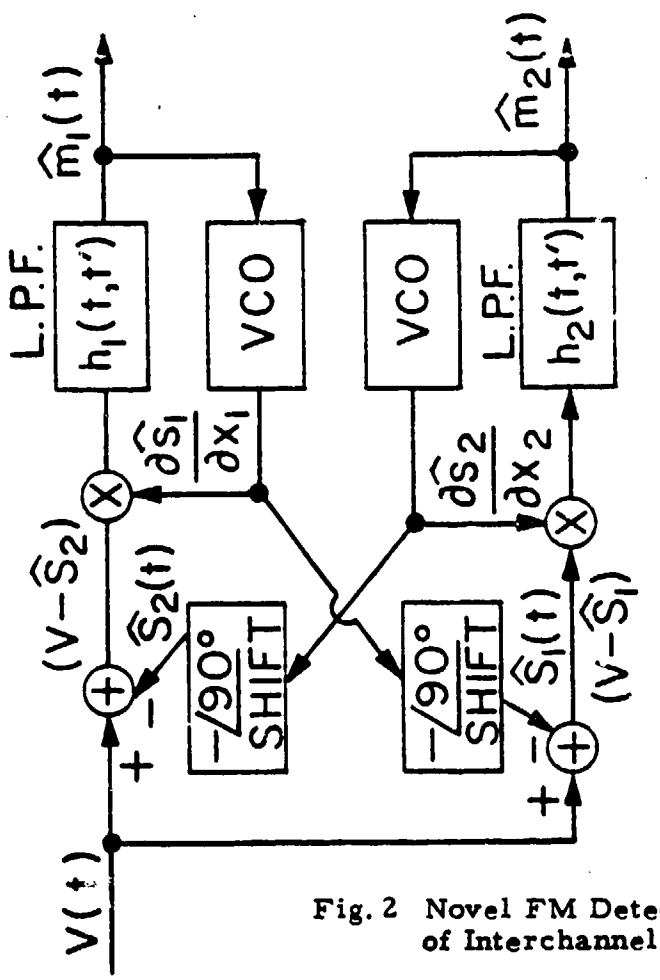

Fig. 2 Novel FM Detector for Suppression of Interchannel Interference

In order to conduct experimental evaluation a physical receiver structure based on the topology of Fig. 2 was constructed. In the physical receiver $h_1(t, \mu)$ and $h_2(t, \mu)$ are replaced by realizable low pass filters of suitable bandwidths as shown in Fig. 3. The principle of operation can be described as follows: assume the input signal consists of a frequency modulated carrier plus a frequency modulated interferer. Phase-locked loop (PLL) #1 locks on to and tracks (by the capture effect) the stronger of the two received FM signals but its voltage controlled oscillator output signal (VCO#1) lags by approximately 90°. An additional 90° phase shift is introduced by phase shifter #2 so that the signal appearing at phase shifter #2's output is 180° out of phase with respect to the stronger received signal. By proper adjustment of the gain constants of summer #2 the stronger received signal is cancelled leaving only the weaker of the two received FM signals at the input to PLL #2. The instantaneous phase of VCO #2 output signal tracks the instantaneous phase of the weaker signal but lags by 90°. An additional 90° phase shift is introduced by phase shifter #1 producing a signal at the output of phase shifter #1 which is 180° out of phase with respect to the weaker of the two received FM signals. The weaker signal can thus be cancelled at summer #1 leaving only the stronger signal appearing at the input to PLL #1. Since this novel detector has two separate outputs -- namely the outputs of the individual phase-locked loops it possesses the capability of demodulating both the stronger and the weaker received signals even though they may be co-channel and share the same frequency band. This is a task impossible with any of the conventional FM detectors since they all obey the well known capture effect.

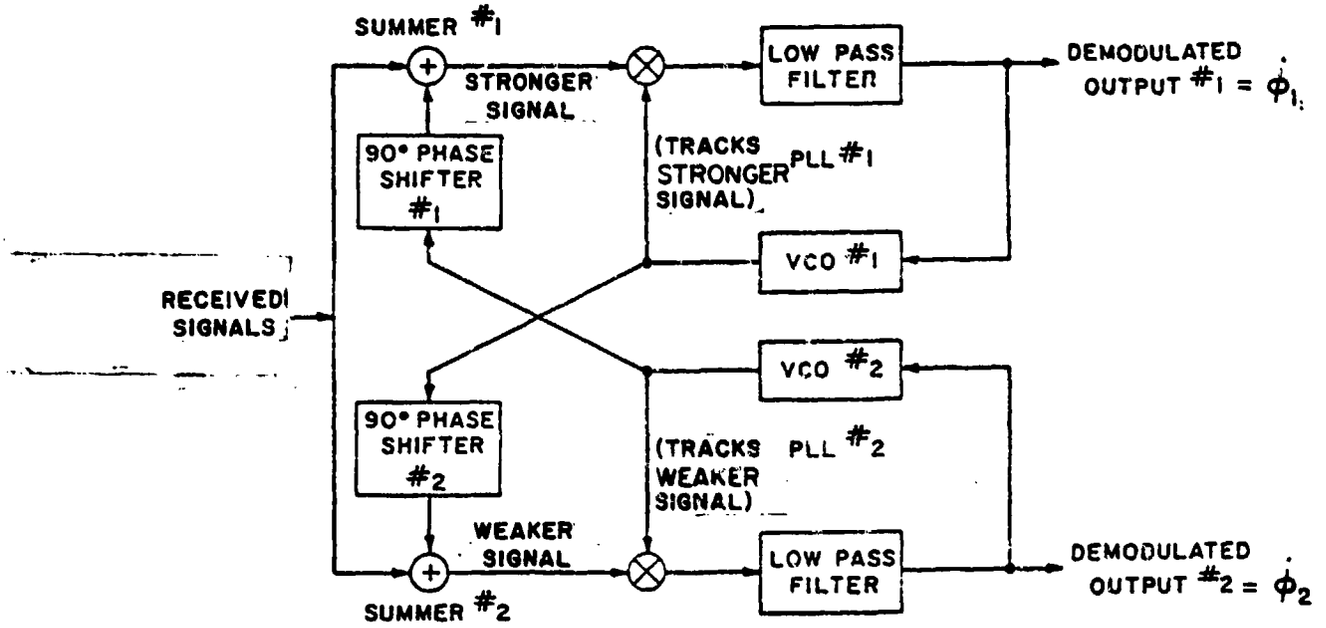

Fig. 3 Block Diagram of Cross Coupled Phase-Locked Loop FM Demodulator

III. Experimental Study

In this section we describe an extensive experimental study conducted on the cross coupled PLL FM demodulator to determine its capabilities and limitations in suppressing numerous types of interfering signals. Fig. 4 describes the experimental set-up used to evaluate the performance of the cross coupled PLL system. The desired FM carrier and interferer were produced by Clarke-Hess function generators. The information signals were simulated by periodic waveforms also obtained from function generators. For those experimental tests requiring random noise a General Radio broadband gaussian noise generator was employed. Its output was filtered by a Collins Radio rectangular shaped mechanical bandpass filter centered at the desired signal's carrier frequency and designed with a bandwidth equal to the desired signal's bandwidth. The FM test signal was used to drive the limiter-discriminator and the novel FM detector simultaneously so that a direct comparison between the two receivers could be made. The limiter discriminator employed was the General Radio pulse count discriminator and the post detection filters used were Krohn-Hite low pass filters with a 4 pole Butterworth design.

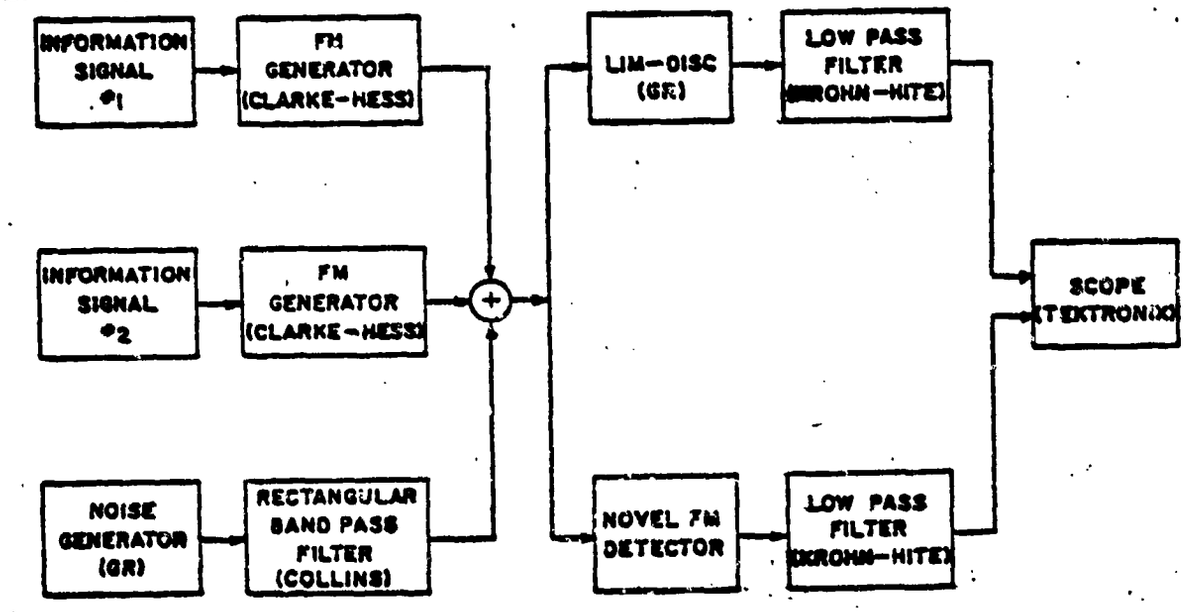

Fig. 4 Block Diagram of Experimental Set-up

In the first experimental test performed the cross coupled PLL receiver was driven by a 200kHz FM sinusoidal carrier plus a co-channel 200kHz FM interferer. No random noise was included in this initial test. The desired carrier was frequency modulated by a 100Hz sinusoid while the interferer was frequency modulated by a 200Hz triangle wave. The peak frequency deviation of both carriers was 8kHz. The interferer to desired carrier amplitude ratio, denoted by the symbol η, was set at 1/2. Each output was filtered by identical 10kHz bandwidth post detection low pass filters which was less than the bandwidth of either PLL. The oscillogram of Fig. 5 describes the response of the novel FM detector and limiter discriminator when simultaneously driven by such a test signal. The upper trace in this oscillogram describes the limiter-discriminator output which, by the capture effect, demodulates the stronger received signal and hence has as its output the 100Hz sinusoid. In addition, it contains noticeable distortion due to the presence of the co-channel interferer. The second trace describes the output of phase-locked loop #1 in the novel FM detector which has been designed to track the stronger carrier and therefore it too has as its output the 100Hz sinusoid. However, as you can see, the distortion due to the presence of the interferer is suppressed considerably. The lower trace describes the output of phase-locked loop #2 which is designed to track the weaker carrier and hence has as its output the 200Hz triangle wave. The results of this figure reveal that the cross coupled PLL can demodulate both the stronger and weaker FM carriers with considerable improvement over the limiter-discriminator even though the received signals are co-channel and share the same frequency. Similar results were obtained for the adjacent channel interferer problem where a separation exists between the two carrier frequencies.

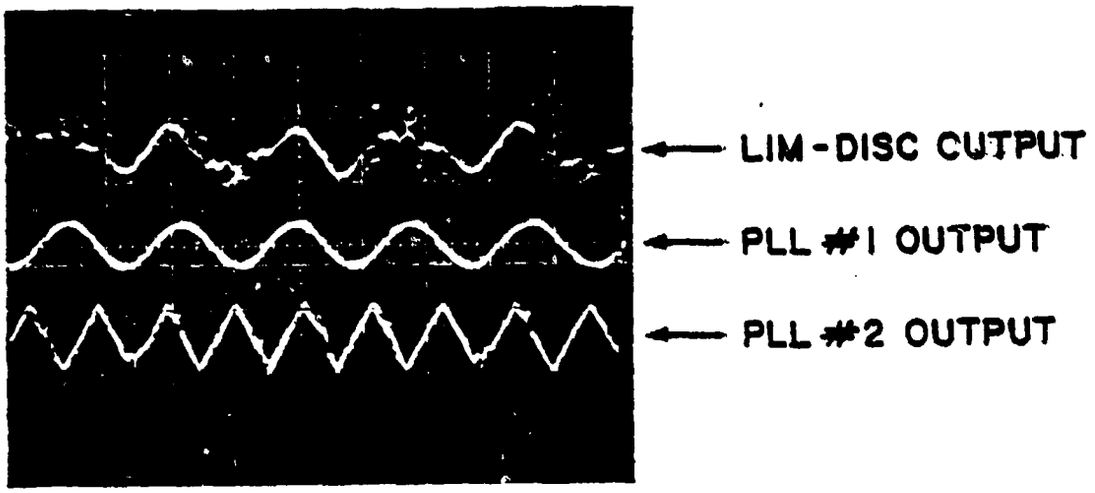

Fig. 5 Response of Lim-Disc. and Novel FM detector with $\eta = 0.5$

In the next experimental test performed the desired FM carrier was corrupted by additive narrowband gaussian noise in addition to the co-channel FM interferer. Fig. 6 describes the results of this test. The stronger received carrier-to-noise ratio (CNR) measured at the input to each detector was 8.7 dB in this test, the weaker CNR was 2.7dB, and the weaker to stronger carrier amplitude ratio, again denoted by the symbol η, was set at 1/2. The results of this oscillogram reveal that the novel detector can demodulate both the stronger and weaker received FM signals despite the rather strong input noise environment. The presence of noise impulses commonly referred to as "clicks" [10] in the detected output signals reveals that both receivers are operating below their FM threshold level.

Similar tests were performed by replacing the periodic information signals with music signals derived from the outputs of two cassette tape recorders. In this test the post detection low pass filter outputs were used to drive an audio power amplifier with a speaker load. Subjective evaluation tests were then performed comparing the limiter-discriminator and novel FM detector outputs. The novel detector successfully separated and tracked the stronger and weaker received carriers over the range $0.1 < \eta < 0.9$ with noticeable improvement over the limiter-discriminator even for the case when the received carrier to noise ratios fall below the FM threshold level.

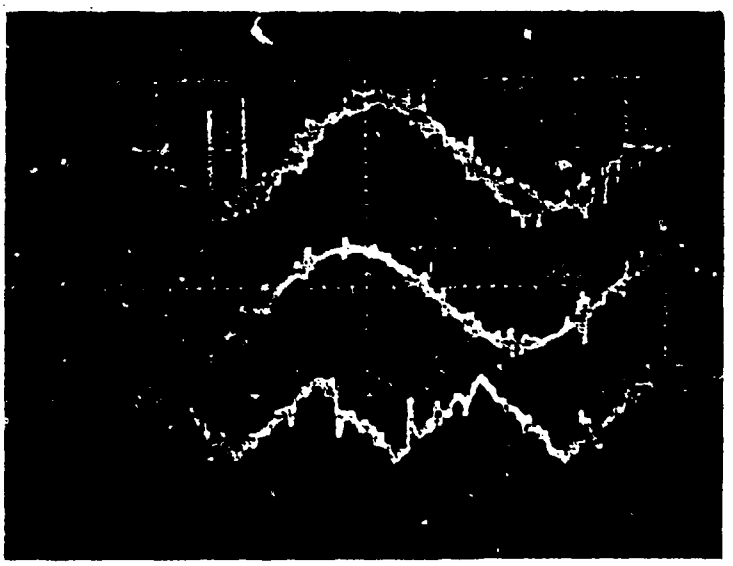

RESPONSE OF LIM-DISC AND NOVEL FM DETECTOR
WITH INTERFERER AND NOISE

η = 0.5 ; CNR = 8.7dB
TIME AXIS : 2MSEC/DIV

Fig. 6 Performance of the novel detector in the presence of noise.

The next test performed relates to the multiple interferer problem, i.e., separating out and demodulating 1 of M co-channel signals. Experimental studies thus far have specialized to the case of M = 3 using the receiver structure shown in Fig. 7. The three input signals used in this test were 455 kHz co-channel FM carriers each with a peak frequency deviation of 7 kHz. The strongest carrier s_1 was a 19V peak-to-peak signal frequency modulated by a 100 Hz sinusoid. The second strongest carrier s_2 was 13V peak-to-peak in amplitude and frequency modulated by a 200 Hz triangle wave and the weakest of the three input signals s_3 was 3V peak-to-peak in amplitude and frequency modulated by a 400 Hz square wave. Each PLL output was filtered by a 6 kHz post detection low pass filter. As can be seen from the block diagram shown the system employs two cross coupled PLL detectors and is designed to operate as follows: PLL #1 is designed to track the strongest carrier s_1 while PLL #2 locks on to and tracks the resultant signal $s_2 + s_3$. The second novel FM detector then separates s_2 and s_3. Similar schemes could be designed for

M larger than three by employing more novel FM detectors. The detected output signals observed are shown in Fig. 8. As can be seen successful demodulation of all three received co-channel signals was achieved. No random noise was included in this test. The distortion appearing in the detected outputs (particularly the weakest channel) is due to the presence of the other co-channel signals.

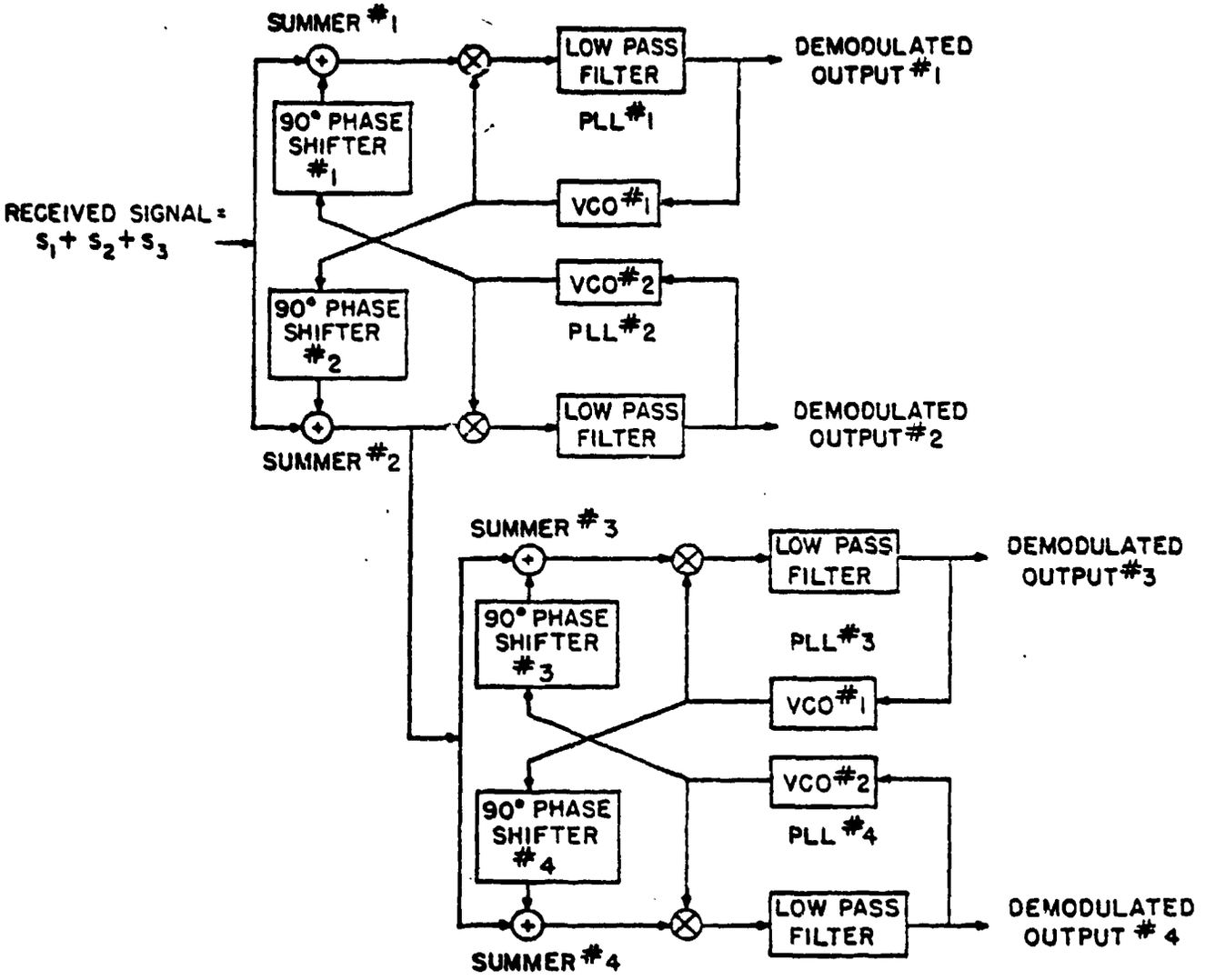

Fig. 7 Receiver structure for detecting 3 co-channel FM signals

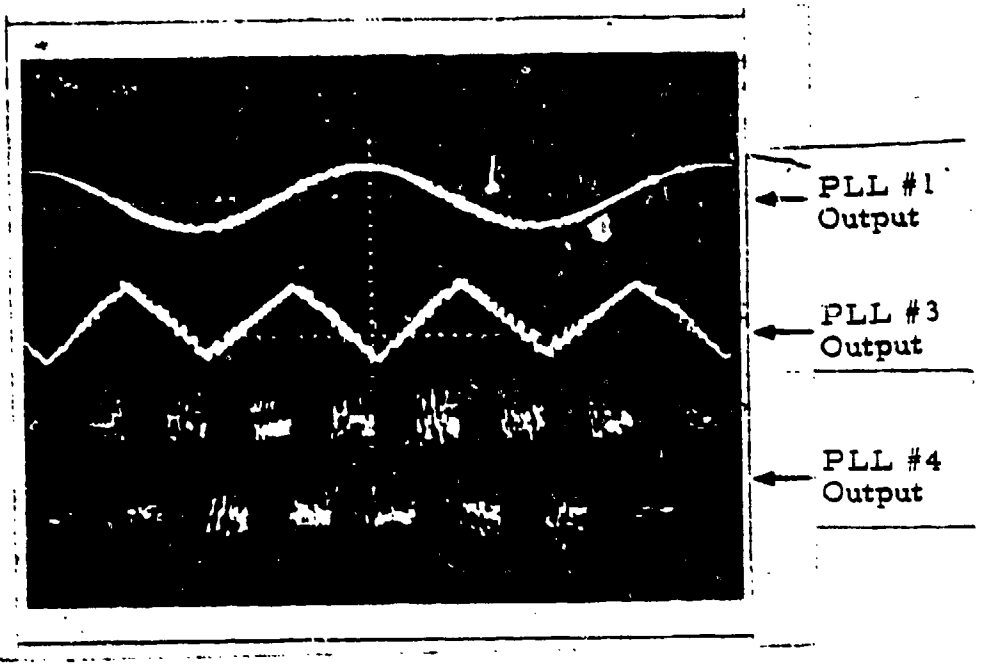

Fig. 8 Detected Outputs for Multiple Interferer Experiment

Cross Coupled PLL with Amplitude Control Loops

The basic cross coupled receiver structure can be modified as shown in Fig. 9 to incorporate amplitude demodulators which estimate the instantaneous amplitude of the two received signals while the phase locked loops simultaneously estimate the instantaneous phase of these input co-channel signals. Such a detector possesses the capability of suppressing a CW, AM, FM, or AM/FM interferer.

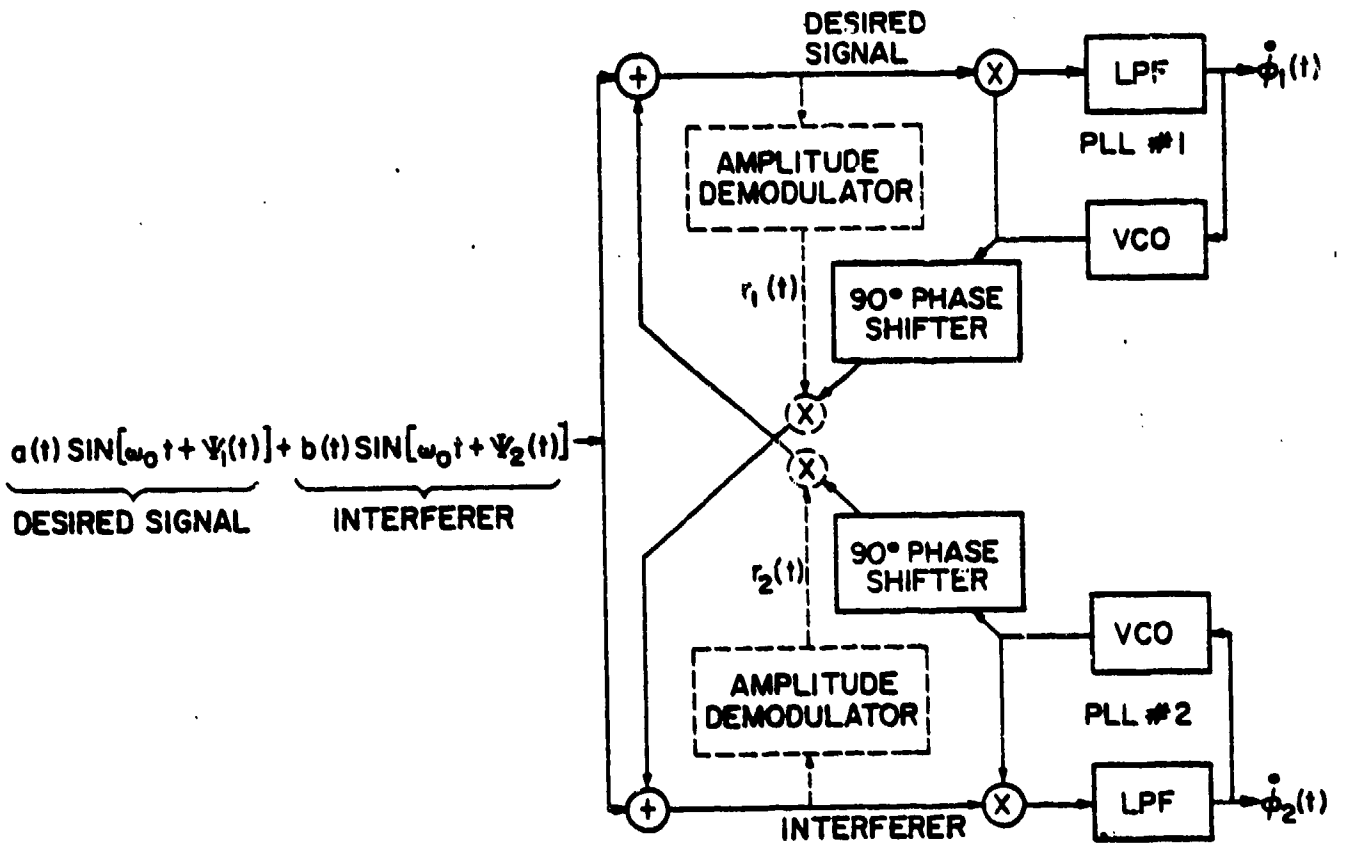

Fig. 9 Block diagram of cross coupled PLL with amplitude control loops

Hardware was also designed and constructed for this cross coupled PLL with amplitude control. A block diagram description is shown in Fig. 10. The design incorporates Tektronix AM/FM function generators for the PLL voltage controlled oscillators. A transistor switch was used for the phase detector and was driven by the VCO constant amplitude square wave output terminal. The quadrature AM/FM sine wave VCO output provides the necessary cancellation signal. Active OP-AMP filters were used for the loop low pass filter. Average envelope detectors were employed for the amplitude control loops. Successful separation and demodulation of the received co-channel signals were obtained for the cases of CW, AM, FM, combination AM/FM, pulsed RF, and noise interferers. With the hardware designed CW interferers could be as much as 20dB stronger than the desired signal while AM/FM interferers with 100% AM modulation index could be accommodated with interferer signal strengths as much as 10dB stronger than the desired signal. Other types of interferers yielded intermediate results between 10 and 20dB.

AM/FM Interferer

An oscillogram revealing a typical result for the AM/FM interferer case is illustrated in Fig. 11. The upper trace in the oscillogram describes the AM/FM interferer frequency modulated by a 100Hz sinusoid with peak frequency deviation of 8kHz and simultaneously amplitude modulated by a 50Hz sine wave. The second trace represents the constant amplitude desired signal frequency modulated by a 200Hz triangle wave also with a peak frequency deviation of 8kHz. Both the interferer and desired carrier frequencies were 200kHz and thus the two received signals were co-channel. The lower two traces describe the demodulated outputs of PLL #1 and PLL #2, respectively, filtered by post detection Krohn-Hite low pass filters of 2kHz bandwidth. The results reveal successful separation and tracking of the input co-channel signals. Both PLLs were second order loop designs.

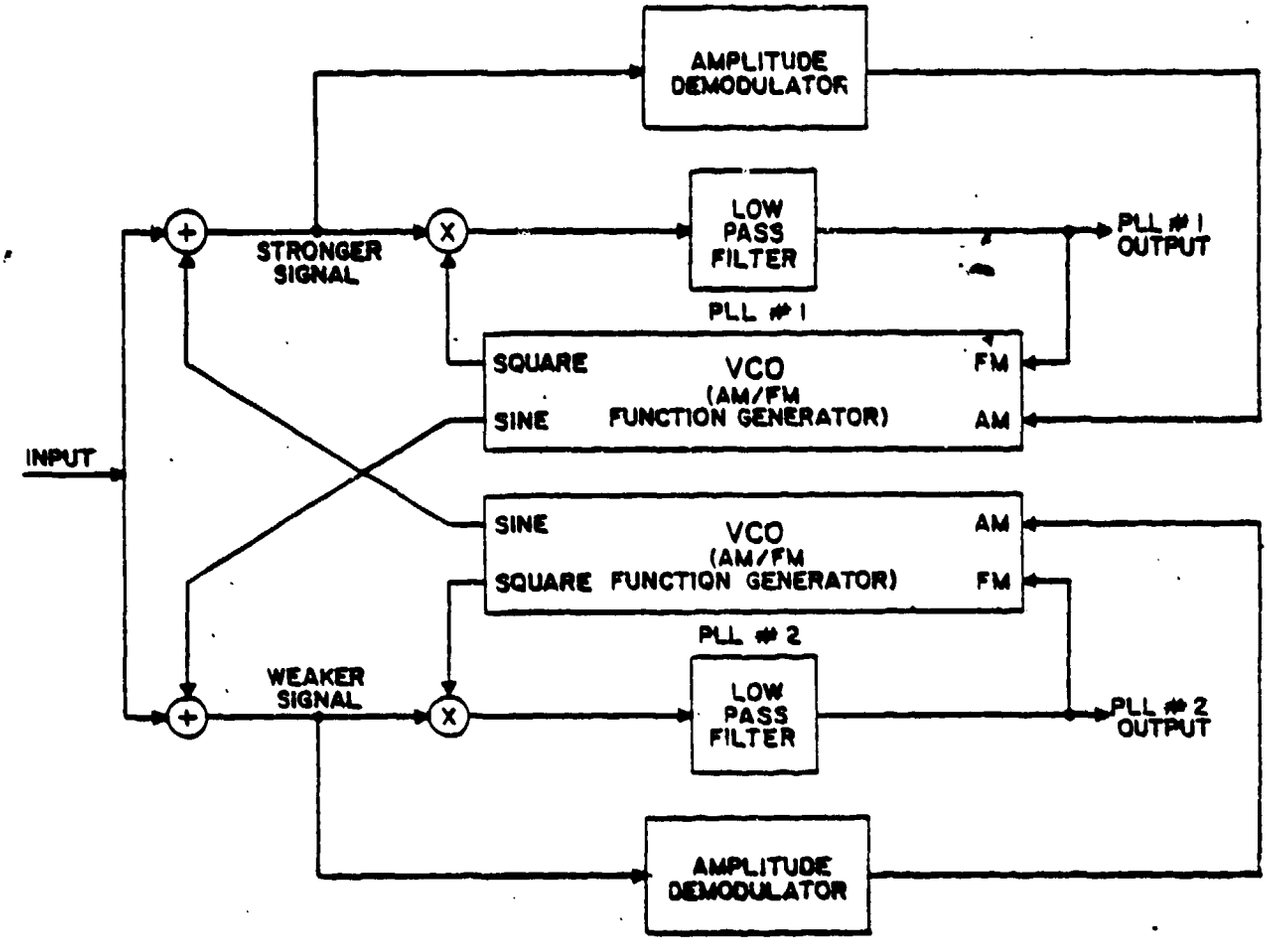

Fig. 10 Block diagram of hardware implementation of cross coupled PLL with amplitude control.

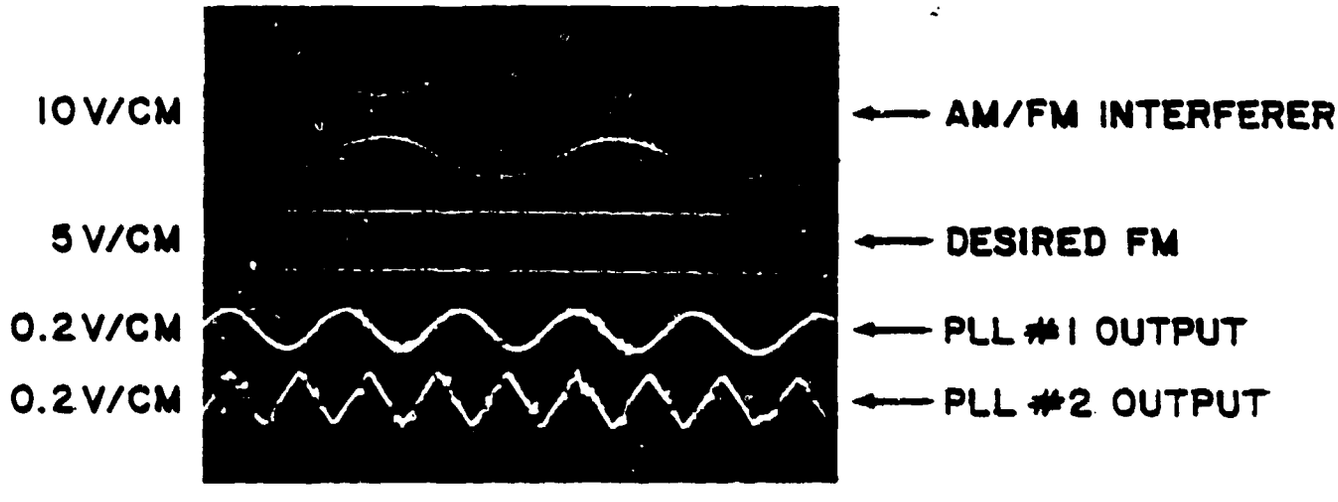

Fig. 11 Oscillogram of cross coupled PLL input and output signals for case of second order loops with AM/FM interferer.

Pulsed RF Interferer

The response of the cross coupled PLL with amplitude control to a pulse RF Interferer is illustrated in Fig. 12. Here the desired signal was frequency modulated by a 200Hz triangle wave. We note from Fig. 12 that during those time intervals when the pulsed RF interval equals zero, PLL #1 output contains the frequency modulation of the received weaker desired FM signal. This occurs because the cancellation of the weaker received signal at the input of PLL #1 is never perfect. The residue left over after cancellation is demodulated by PLL #1 accounting for the PLL #1 output shown.

Noise Jammer

The response of the cross coupled PLL with amplitude control is shown in the oscillogram of Fig. 13. In this case random gaussian noise of 20kHz bandwidth is used to frequency modulate a carrier. The response of the demodulator demonstrates once again successful separation and demodulation of each received co-channel FM signal.

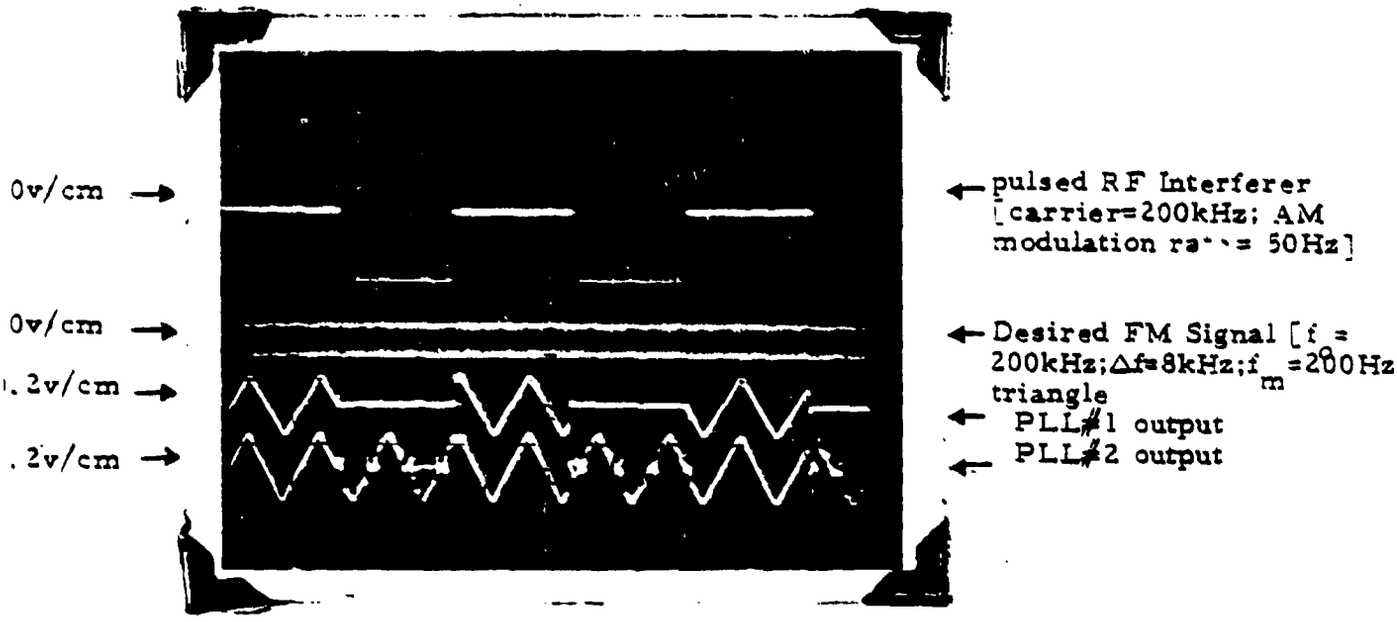

Fig. 12 Response to Pulsed RF Interferer

Generation of Noise Jammer

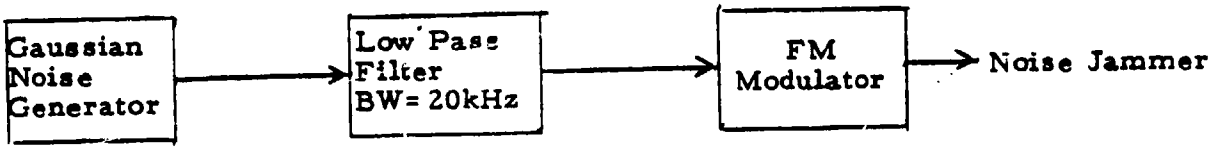

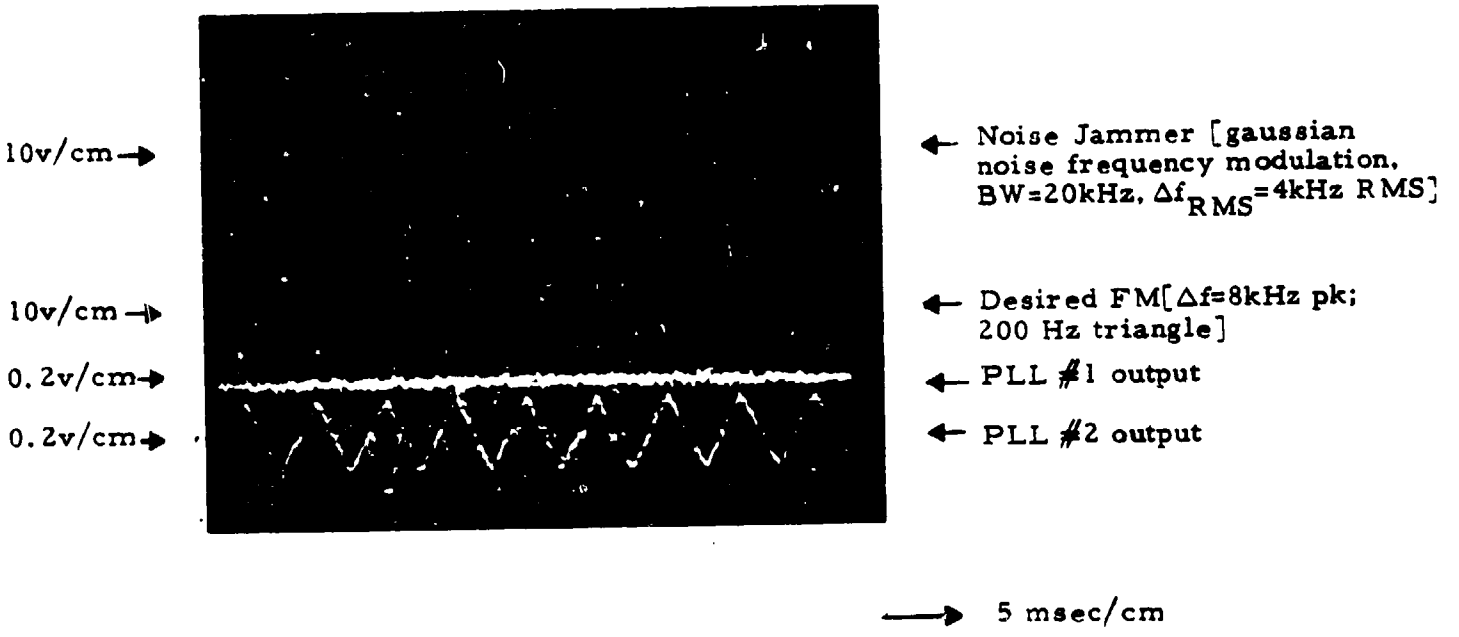

Fig. 13 Response of cross coupled PLL with amplitude control to FM signal corrupted by a noise jammer

IV. Computer Simulation Study of Transient Acquisition Behavior of the Cross Coupled PLL Receiver

In order to determine the PLL parameters which insure successful acquisition and separation of the two received FM signals, a theoretical analysis of the transient acquisition behavior of the cross-coupled PLL system was conducted. Such an analysis was carried out taking into account PLL order, relative bandwidths of the two PLLs, low pass loop filter parameters, amplitude ratio of the two received FM carriers, frequency deviation, and FM modulation index of the individual carriers.

The normalized defining coupled nonlinear differential equations for the novel FM detector of Fig. 3 are derived in Appendix B and are given below:

$$\frac{d\varphi_1}{d\tau} = \alpha_1[\sin(\psi_1 - \varphi_1) + \eta \sin(\psi_2 - \varphi_1) - \eta \sin(\varphi_2 - \varphi_1)] * h_{L1}(\tau) \tag{9}$$

$$\frac{d\varphi_2}{d\tau} = \alpha_2[\sin(\psi_1 - \varphi_2) + \eta \sin(\psi_2 - \varphi_2) - \sin(\varphi_1 - \varphi_2)] * h_{L2}(\tau) \tag{10}$$

where

ψ_1 and ψ_2 denote the phase modulation of the stronger and weaker received FM carriers respectively.

φ_1 and φ_2 represent, respectively, the phase modulation of VCO #1 and VCO #2.

$\alpha_1 = \frac{\omega_{H1}}{\omega_N}$ where ω_{H1} denotes the equivalent first order loop static hold-in-range of PLL #1 and

ω_N denotes some selectable "normalization frequency".

$\alpha_2 = \frac{G_2}{G_1}\alpha_1$ where G_1 and G_2 are, respectively, the dc gains of the PLL low pass filters.

η denotes the ratio of the weaker to stronger carrier amplitudes and $h_{L1}(t)$ and $h_{L2}(t)$ are the impulse responses of each PLL low pass loop filter.

Digital computer solutions of these equations were obtained for the cases of (a) first order loops with a CW interferer, (b) first order loops with a frequency offset CW interferer, (c) second order loops with a frequency offset interferer, and (d) second order loops with a frequency modulated interferer. In all of the above cases, the desired signal was frequency modulated by a sinusoid. For each case mentioned the range of loop parameters, i.e., the "stability region" over which the cross-coupled PLL demodulator can successfully separate and demodulate the two received co-channel signals was determined. Such stability regions provide useful design rules.

One example of the transient acquisition response of the cross coupled PL system is illustrated in Figs. 14(a) and 14(b) for the case of first order loops with a constant frequency offset CW interferer. Here the filtered outputs (y_1^* and y_2^*) for each PLL obtained by solving Eqs. (9) and (10) on the PDP 11/60 digital computer are plotted versus normalized time $\tau = \omega_N t$. Each PLL output $\dot{\phi}_1$ and $\dot{\phi}_2$ is filtered by a four pole Butterworth post detection low pass filter of normalized bandwidth 2.5 to produce y_1^* and y_2^*, respectively. The normalization frequency (ω_N) was selected to be ω_{m2}. This corresponds to the modulation rate of the weaker carrier, frequency modulated by a sinusoid with FM modulation index (β) of 10 and peak frequency deviation ($\Delta\omega_2$) of 10. The normalized frequency offset used for the CW interferer was 0.5 while its amplitude was twice as strong as the weaker carrier ($\eta = 1/2$). Fig. 14(a) reveals a set of loop parameters ($\alpha_1 = 8$, $\alpha_2 = 60$) which provides for successful acquisition, separation, and demodulation of the two received co-channel signals. Decreasing α_1 by less than 10 percent to $\alpha_1 = 7.5$ reveals unsuccessful tracking. Similar transient responses show that for $\alpha_2 = 60$ unsuccessful tracking occurs for any α_1 less than 7.5. The coordinates ($\alpha_1 = 8$, $\alpha_2 = 60$) represent, therefore, a point on the boundary separating successful tracking and demodulation from an unsuccessful result. A search was made for the complete boundary for several types of interferers by varying the loop parameters one at a time in a systematic manner and observing the transient responses similar to those of Figs. 14(a) and 14(b) on a CRT interactive graphics terminal.

Fig. 15(a) reveals a typical result for a first order PLL design with a single CW interferer located at the center of the IF frequency band, i.e., no frequency offset. The weaker signal was again frequency modulated by a sinusoid with an FM modulation index equal to 10. The PLL loop parameters α_1 and α_2 shown in Fig. 15(a) were normalized to the modulation frequency of this sinusoid, i.e., ω_N was

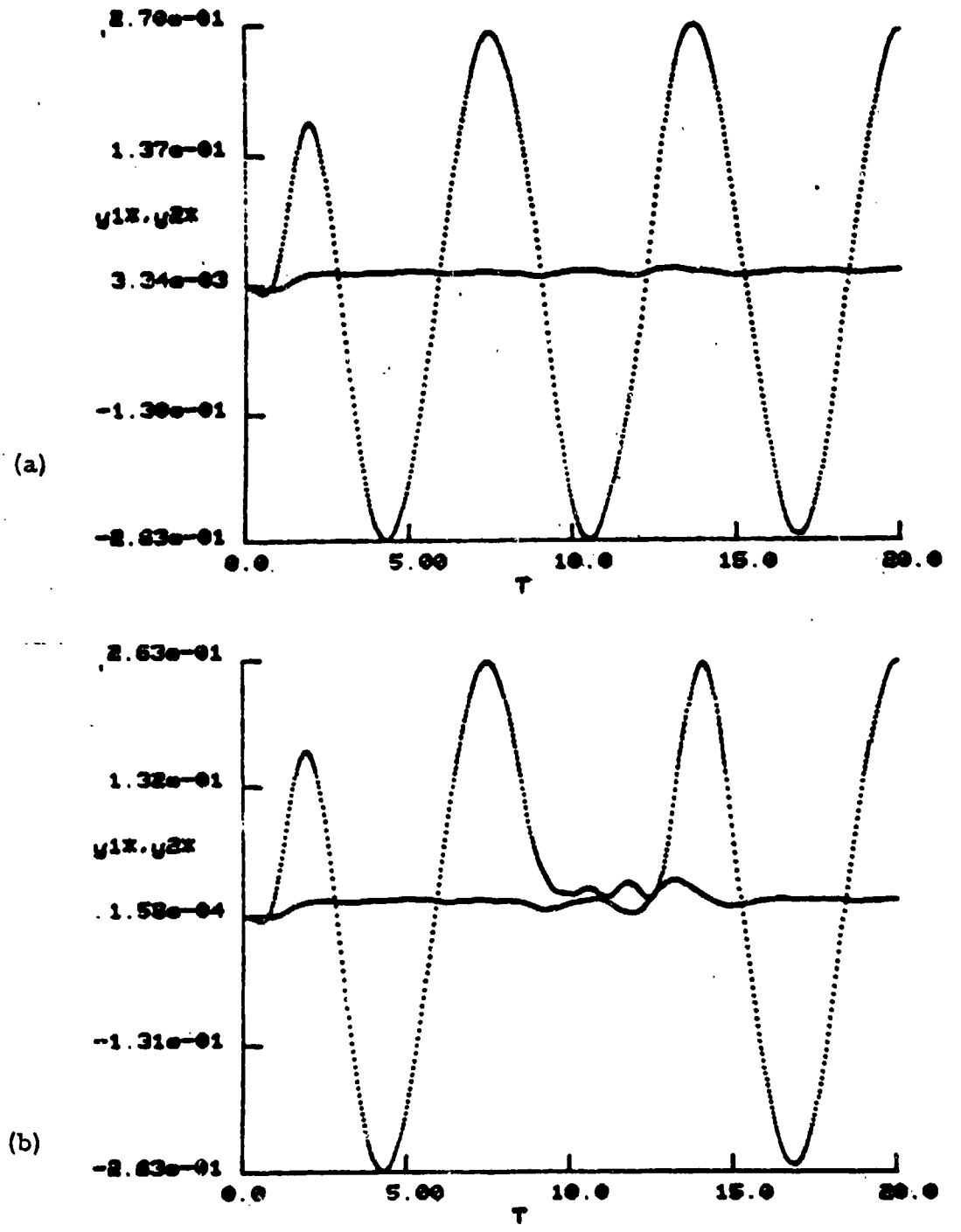

Fig. 14 Transient acquisition response for case of sinusoidally modulated FM carrier corrupted by frequency offset CW interferer ($\Delta\omega = 0.5$). Solid line = PLL #1 output. Dotted line = PLL #2 output.

(a) Loop constants $\alpha_1 = 8$, $\alpha_2 = 60$

(b) Loop constants $\alpha_1 = 7.5$, $\alpha_2 = 60$

again selected to be ω_{m2}. For successful separation and demodulation, PLL #2's steady state bandwidth, $\eta\alpha_2$, must be designed to lie above the solid curves of Fig. 15(a). Since the hold-in-range or equivalently the bandwidth of PLL #2 is proportional to the received signal amplitude, the smaller the value of η the larger must be the dc loop gain for PLL #2. In fact, the minimum value permitted for PLL #2's hold-in-range, $\eta\alpha_2$, must exceed the peak frequency deviation, $\Delta\omega_2 = \beta\omega_{m2}$, of the weaker signal.

Hence,

$$\alpha_{2_{min}} = \frac{\beta\omega_{m2}}{\eta}$$

This agrees well with the values of α_2 with $\alpha_1 = 0$ shown in Fig. 15(a). Experimental results obtained on an experimental model designed to accommodate sinusoidal carriers are also shown on Fig. 15(a) for the case of $\eta = 0.5$ and reveal good agreement with the theoretical result. The curves shown in Fig. 15(a) approximately coalesce to one single curve if the vertical axis of Fig. 15(a) is changed to $\eta\alpha_2$ as in Fig. 15(b). The slope of the linear portion of this curve is approximately 2 and its vertical axis intersection corresponds to $\Delta\omega_2$ peak, the peak frequency deviation of the desired FM signal. Fig. 15(b) provides the following useful design rule: for successful tracking of a desired FM signal corrupted by a stronger CW interferer, design the first order PLL hold-in-ranges such that $\eta\alpha_2 > 2\alpha_1 + \Delta\omega_2$ peak. The physical insight offered by this theoretical result is that PLL #1's bandwidth, α_1, must be designed to be narrow, relative to the bandwidth of PLL #2, so that VCO #1 may reject a good portion of the signal energy of the received desired FM signal and thus develop a good estimate of the instantaneous phase of the CW interferer and provide the necessary cancellation signal to summer #2 (see Fig. 3). Fig. 15(c) describes similar results for the 1st order loop and CW interferer with β as a parameter.

Figs. 16(a) and 16(b) describe the stability regions for the case when the carrier frequency of the CW interferer is offset from the center of the IF band. Fig. 16(a) reveals that for the first order loop design the stability regions are quite narrow and not much frequency offset can be allowed if successful separation and demodulation of the two received signals is to be achieved. This result seems plausible when we consider the fact that for a first order PLL design a steady state phase error is present in the VCO output signal when the PLL input signal is frequency offset from the VCO free running rest frequency thus making cancellation of the interferer difficult.

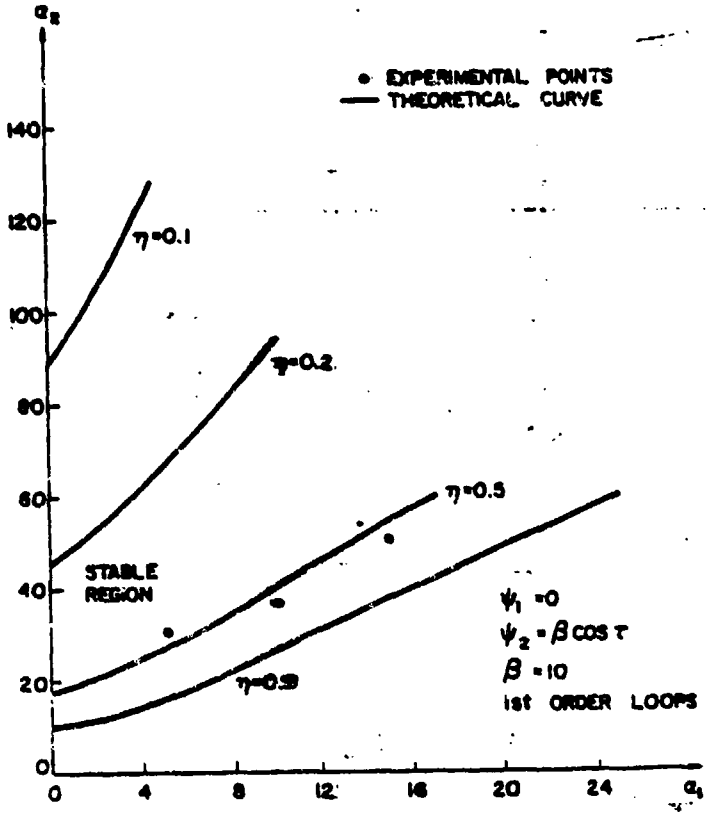

15(a)

FIRST ORDER LOOPS WITH CW INTERFERER

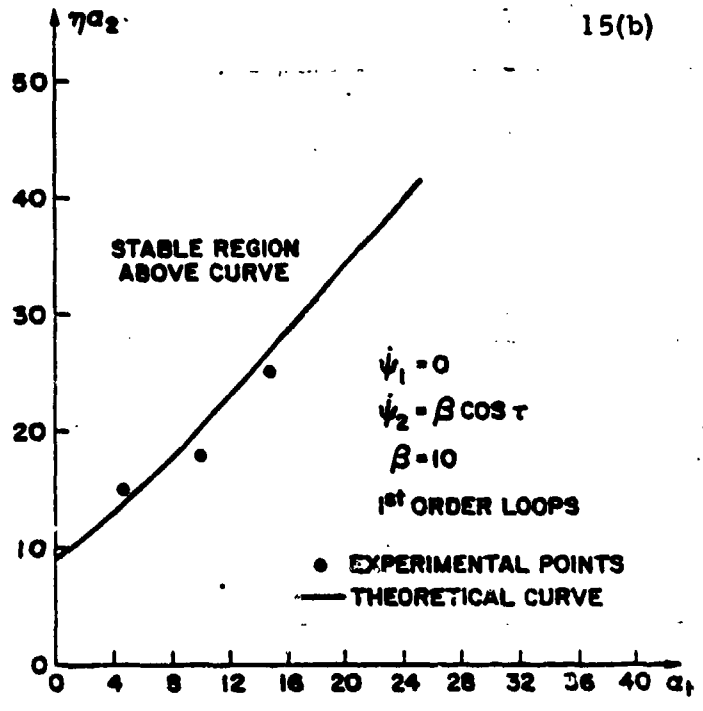

15(b)

FIRST ORDER LOOPS WITH CW INTERFERER

Fig. 15 Stability regions for the cross coupled PLL receiver for the case of first order loops and CW interferer

(a) Loop parameters α_2 versus α_1 with η as parameter

(b) Loop parameters $\eta\alpha_2$ versus α_1

(c) Loop parameters α_2 versus α_1 with β as parameter

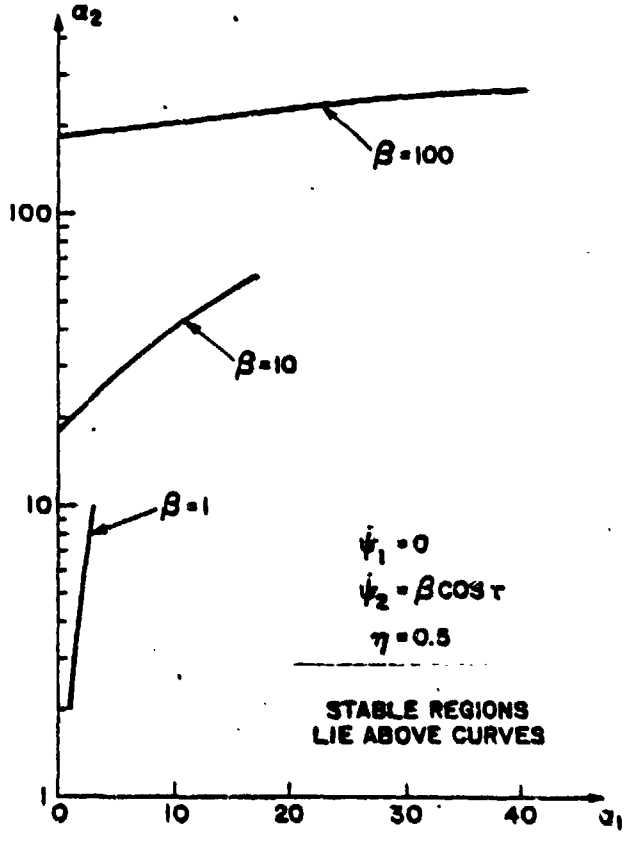

15(c)

A second order loop with a low pass loop filter consisting of constant plus integral control provides the necessary dc control voltage to allow PLL #1's voltage controlled oscillator to re-center itself and phase lock to the offset interferer with no phase error. This permits the second order loop design to accommodate carrier frequency offsets as large as the peak frequency deviation of the interferer as Fig. 16(b) reveals. In these stability region plots the Laplace Transform transfer function of the PLL low pass loop filter takes on the form $H_L(s) = 1 + K/s$.

Figs. 17(a) and 17(b) describe the stability region locations for the case of second order loops with sinusoidal modulation on both carriers. The parameters present in this computer analysis include $\alpha_1, \alpha_2, \omega_{m1}, \omega_{m2}, K_1, K_2, \beta_1, \beta_2$, and η and represents a rather large list. Hence a complete set of cross sectional stability region plots is virtually impossible to obtain. However, the results obtained for first order loops and CW interferers where the effect of η and β were examined (see Fig. 15(a) and 15(c)) are useful even here to obtain at least a qualitative feel for where the parameters should be designed for those cases not covered by Figs. 17(a) and 17(b).

Transient Acquisition Behavior of Cross Coupled PLL with Amplitude Control

A computer simulation study examining the transient acquisition behavior of the cross coupled PLL with amplitude control shown in Fig. 9 was also conducted. The normalized defining coupled nonlinear differential equations for this system were derived and are given below:

$$\text{RECEIVED SIGNAL} = A \sin\left[\omega_0 t + \psi_1(t)\right] + \eta A \sin\left[\omega_0 t + \psi_2(t)\right]$$

$$\dot{\phi}_1 = \alpha_1\left[\sin(\psi_1-\phi_1)+\eta\sin(\psi_2-\phi_1)-r_2(\tau)\sin(\phi_2-\phi_1)\right] * \ell_{L1}(\tau)$$

$$\dot{\phi}_2 = \alpha_2\left[\sin(\psi_1-\phi_2)+\eta\sin(\psi_2-\phi_2)-r_1(\tau)\sin(\phi_1-\phi_2)\right] * \ell_{L2}(\tau)$$

$$\dot{r}_1(\tau)+\alpha_1 r_1(\tau) = \alpha_1\left\{\left[\cos\psi_1+\eta\cos\psi_2-r_2\cos\phi_2\right]^2+\left[\sin\psi_1+\eta\sin\psi_2-r_2\sin\phi_2\right]^2\right\}^{1/2}$$

$$\dot{r}_2(\tau)+\alpha_2 r_2(\tau) = \alpha_2\left\{\left[\cos\psi_1+\eta\cos\psi_2-r_1\cos\phi_1\right]^2+\left[\sin\psi_1+\eta\sin\psi_2-r_1\sin\phi_1\right]^2\right\}^{1/2}$$

FIRST ORDER LOOPS WITH
CONSTANT FREQUENCY OFFSET INTERFERER

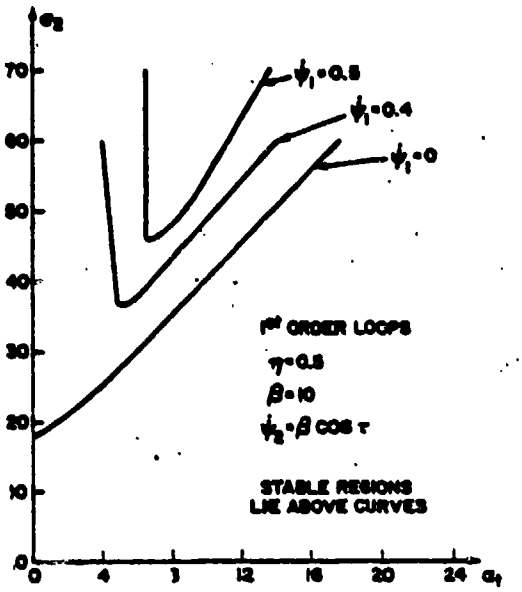

16(a)

SECOND ORDER LOOPS WITH
CONSTANT FREQUENCY OFFSET INTERFERER

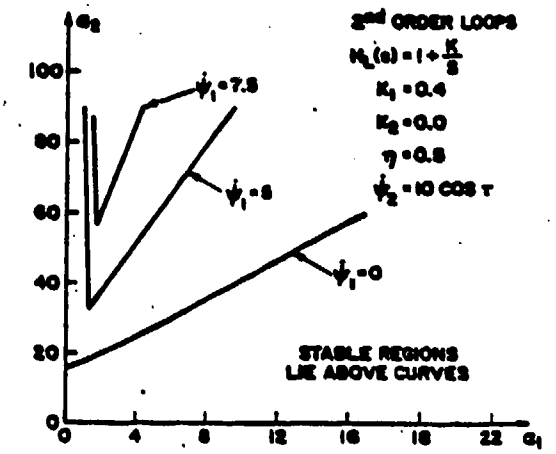

16(b)

Fig. 16 Stability regions for case of frequency offset CW interferer

(a) first order loops
(b) second order loops

SECOND ORDER LOOPS WITH FM INTERFERER

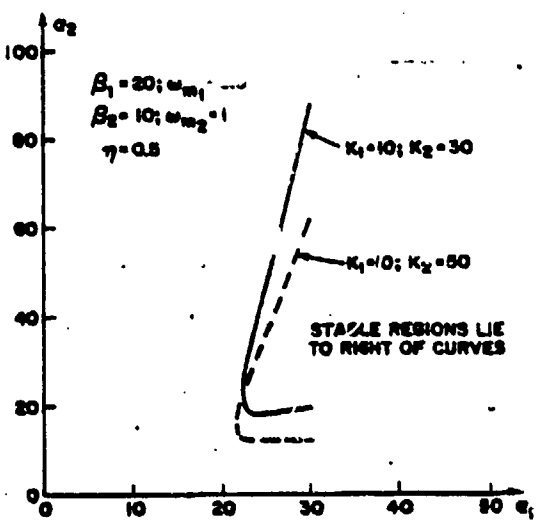

17(a)

SECOND ORDER LOOPS WITH FM INTERFERER

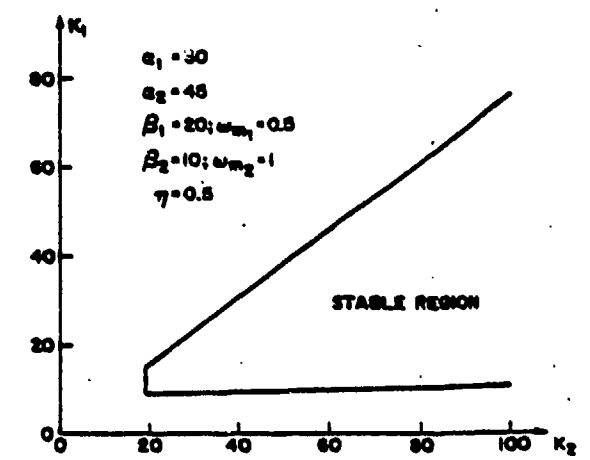

17(b)

Fig. 17 Cross coupled PLL stability regions for case of second order loops and FM interferer

(a) loop parameters α_2 versus α_1 with low pass loop filter constants K_1, K_2 as parameters
(b) loop parameters K_1 versus K_2

Here ψ_1 and ψ_2 denote the instantaneous phases of the stronger and weaker received signals. η denotes the weaker to stronger amplitude ratio, $\dot{\phi}_1$ and $\dot{\phi}_2$ the demodulated outputs of each PLL, α_1 and α_2 represent the equivalent first order loop static hold-in-ranges, r_1 and r_2 denote the output of the amplitude demodulator, and a_1, a_2 are the 3dB bandwidths of the amplitude control loops. Both the alphas and the a's are normalized to ω_{m2}, the modulation frequency of the weaker FM carrier. h_{L1} and h_{L2} are the impulse responses of each PLL low pass loop filter.

Digital computer solutions of these coupled differential equations were obtained on the PDP 11/60 for numerous first and second order loop designs and various input signal conditions. For each case the range of loop parameters, i.e., the "stability region" over which the cross-coupled PLL demodulator can successfully separate and demodulate the two received co-channel signals was determined. Such stability regions provide useful design rules. The next group of figures describe the techniques used to generate these stability regions.

Transient responses of the unfiltered PLL outputs are illustrated in Fig. 18 for the case of an FM interferer.

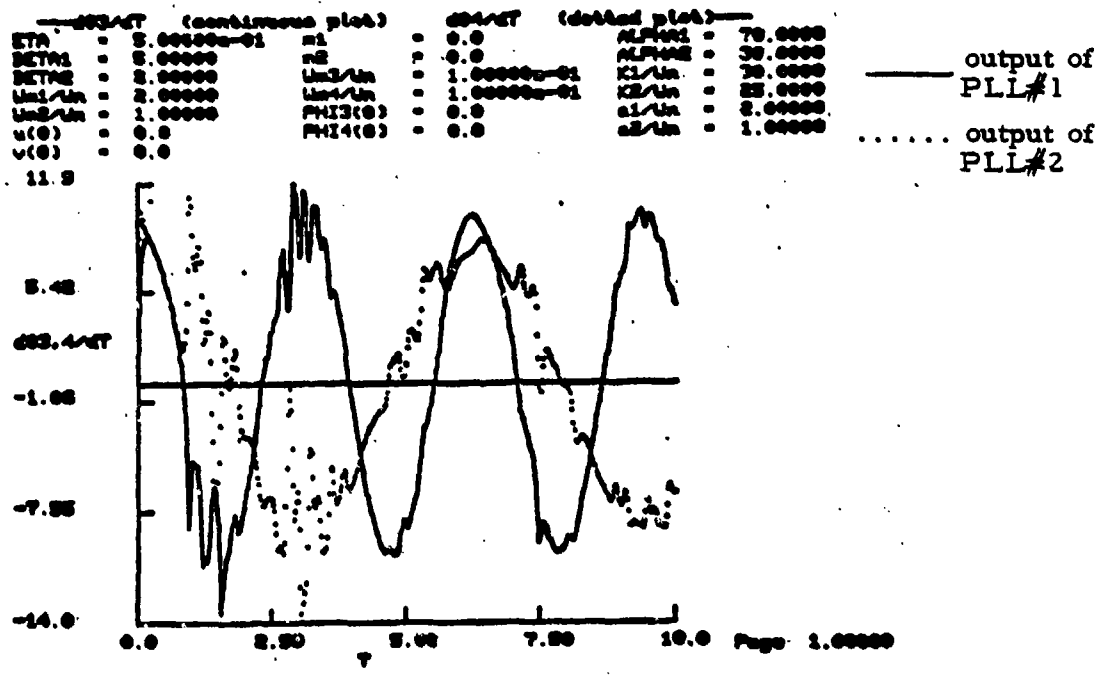

Fig. 18 Response of cross coupled PLL with amplitude control loops to two received co-channel FM signals obtained from computer simulation study.

Here we plot the demodulated output waveforms $\dot{\varphi}_1$ and $\dot{\varphi}_2$ versus normalized time τ. The output of PLL #1 is represented by the solid line and the output of PLL #2 is shown dotted. These results come directly from the CRT interactive graphics terminal. Here the weaker carrier was frequency modulated by a 1 rad./sec. sinusoid while the stronger was frequency modulated by a 2 rad./sec. sinusoid. All the loop bandwidths, integrator constants, and time axis τ shown here are normalized to ω_{m2}, the modulation frequency of the weaker carrier. To go from normalized time τ to real time t one must divide the τ axis by ω_{m2}. Hence for a 1 krad./sec. modulation signal this 0 to 10 second interval indicated on the normalized time axis would actually be 0 to 10 msec in real time. Similarly the normalized loop hold-in-range parameters α_1, α_2 shown here as 70 and 30 must be multiplied by the normalization frequency ω_{m2} and hence in this example would actually be 70 and 30 krad./sec. These transient waveforms reveal that this selection of loop parameters yields successful separation and tracking of the two input FM signals. It is possible that a change in loop parameters and/or a change in input signal conditions will yield unsuccessful results. A Fourier transform of this waveform in its steady state region was computed and is shown in Fig. 19.

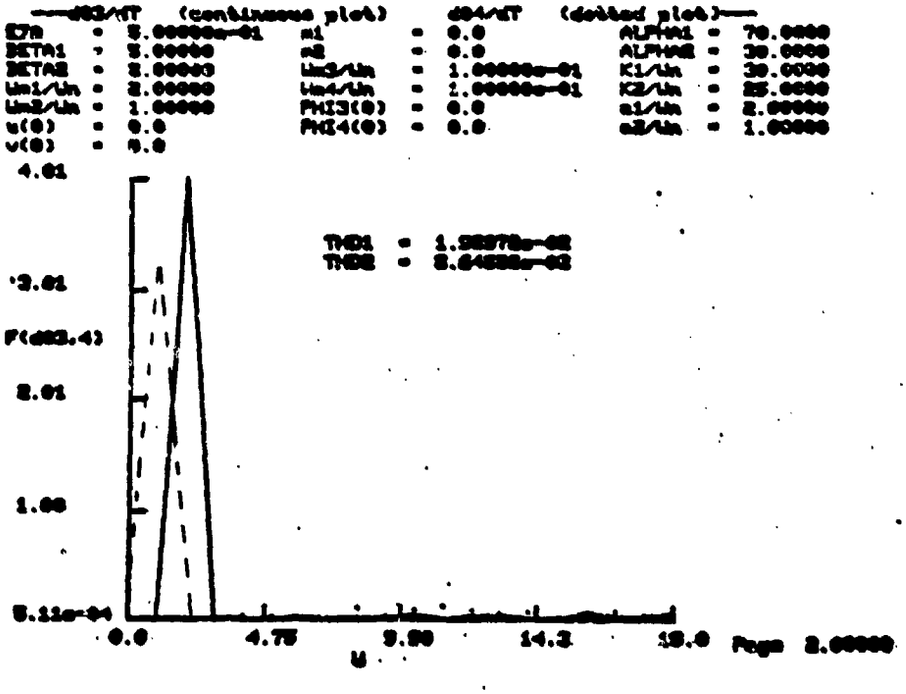

Fig. 19 Fast Fourier Transform of PLL outputs (Solid line = PLL #1 output; Dottled line = PLL #2 output)

The solid line denotes the spectrum of PLL #1 output while the dotted corresponds to the spectrum of PLL #2 output. Here we see the 2 rad./sec. component appearing at the output of PLL #1 which is tracking the stronger carrier and the 1 rad./sec. component appearing at the output of PLL #2 which is demodulating the weaker input FM signal. The remaining terms represent distortion over a 20 rad./sec. baseband bandwidth. A computation of total harmonic distortion (THD) was made for each PLL output signal over this baseband bandwidth and the results are given by the numbers labeled THD 1 and 2 on this figure. This process was repeated for numerous loop parameters and several different input signal conditions. So-called "regions of stability", i.e., regions where successful acquisition and tracking of the two received signals is achieved were obtained. This "stability region" was defined as that set of loop parameters which yields a THD < 20% on both PLL outputs. Examples of such regions appear in the next group of figures.

Fig. 20 reveals the stability region for the case of 2nd order loops and an FM interferer, with the loop hold-in-ranges α_1, α_2 as variables.

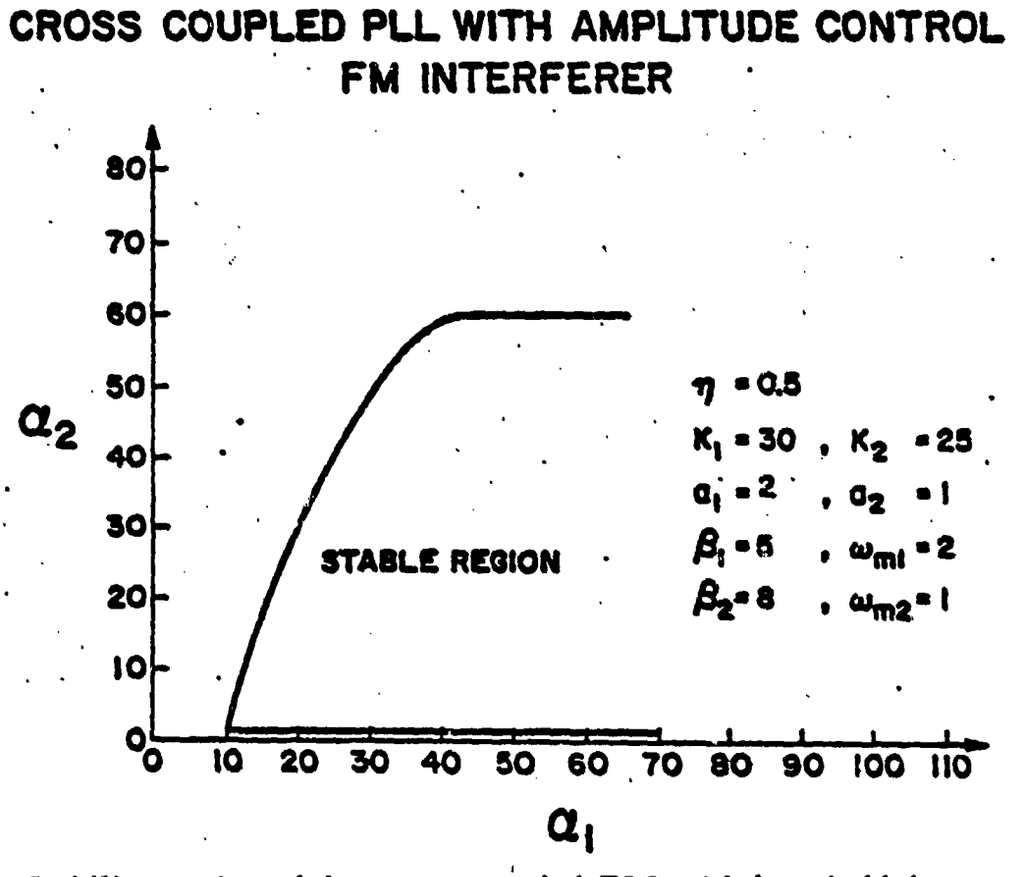

Fig. 20 Stability region of the cross coupled PLL with loop hold-in-ranges (α_1, α_2) as variables.

All other loop parameters are fixed at the normalized values shown. The low pass loop filter was selected to be a constant plus integral control. The symbol K denotes the normalized integrator constants. a_1 and a_2 again denote the normalized 3dB bandwidths of the amplitude control loops, β_1 and β_2 the FM modulation indices of the input signals, ω_{m1} and ω_{m2} the normalized modulation rates, and η denotes the weaker to stronger carrier amplitude ratio. The border of the stability region represents a rather sharp boundary. Just outside the border the THD is much greater than 20% and separation of the two received signals is for all practical purposes not accomplished.

Fig. 21 reveals the sensitivity of the stability region with respect to low pass loop filter integrator constants K_1 and K_2.

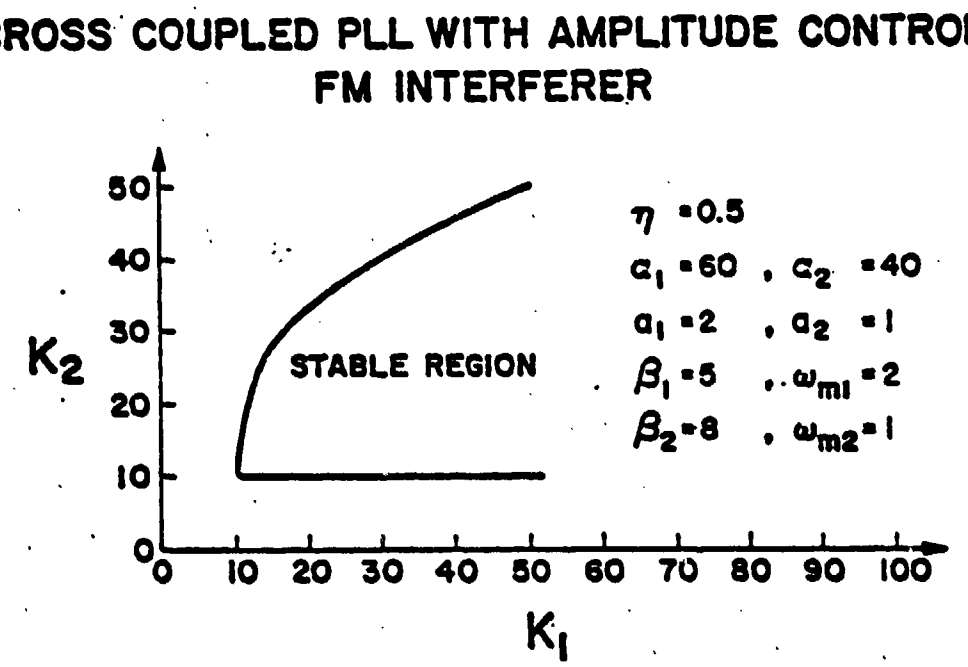

Fig. 21 Stability region of the cross coupled PLL with amplitude control loop with low pass filter constants (K_1, K_2) as variables.

Fig. 22 is the result when the normalized amplitude control loop bandwidths a_1, a_2 are selected as the variables.

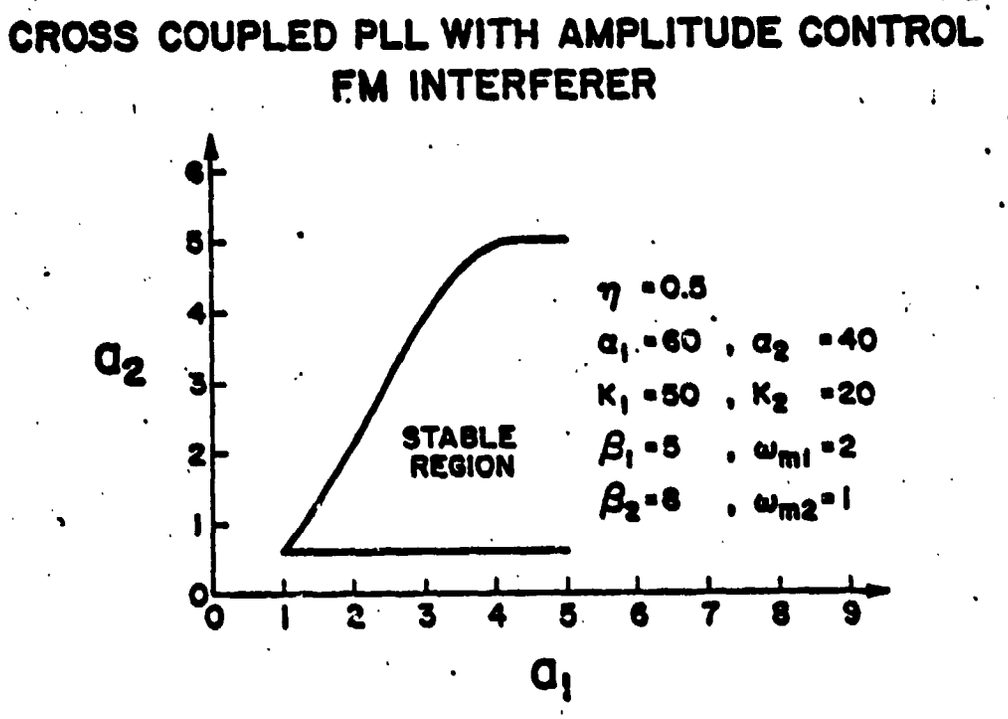

Fig. 22 Stability of cross coupled PLL with amplitude control loop 3dB bandwidths (a_1, a_2) as variables.

The large list of loop parameters - namely hold-in-ranges α_1, α_2; low pass loop filter integrator constants K_1, K_2, and amplitude control loop bandwidths a_1, a_2; as well as the large list of input signal parameters: amplitude ratio η, FM modulation indices β_1, β_2, and FM modulation rates ω_{m1}, ω_{m2} makes it unfeasible to obtain complete cross sectional plots from this computer simulation study. The specific cases discussed here should at least provide a starting point for a successful design.

One of our future objectives includes seeking that set of loop parameters which is insensitive, i.e., robust, with respect to input signal conditions. Such a design would be useful in suppressing a variety of interfering signals without the need to switch loop parameters.

V. Theoretical Models

In this section theoretical models of the cross coupled PLL demodulator are presented. Analysis is restricted here to the case of first order loops, constant amplitude input FM signals, and pre-adjusted summer constants. For this case the defining coupled nonlinear differential equations for the system of Fig. 3 reduce to:

$$\dot{\varphi}_1 = \alpha_1[\sin(\psi_1 - \varphi_1) + \eta \sin(\psi_2 - \varphi_1) - \eta \sin(\varphi_2 - \varphi_1)] \tag{11}$$

$$\dot{\varphi}_2 = \alpha_2[\sin(\psi_1 - \varphi_2) + \eta \sin(\psi_2 - \varphi_2) - \sin(\varphi_1 - \varphi_2]$$

where ψ_1 and ψ_2 denote the instantaneous phases of each received FM signal, $\dot{\varphi}_1$ and $\dot{\varphi}_2$ the PLL outputs, η represents the weaker to stronger received carrier amplitude ratio, and α_1, α_2 the hold-in-ranges (or equivalently 3dB closed loop bandwidths) of the first order phase-locked loops.

The desired solutions of Eq. (11) would be a decoupling of the two differential equations, i.e., we would like $\dot{\varphi}_2 = \dot{\psi}_2$ and $\dot{\varphi}_1 = \dot{\psi}_1$ and the purpose of our theoretical analysis here is to find out under what conditions this is possible or approximately true. To accomplish this we rewrite Eq. (11) in terms of the loop phase errors θ_1 and θ_2 defined as follows:

$$\begin{aligned} \theta_1 &= \psi_1 - \varphi_1 \\ \theta_2 &= \psi_2 - \varphi_2 \end{aligned} \tag{12}$$

Rearranging Eq. (11) in terms of ψ_1, ψ_2, θ_1, and θ_2 and eliminating φ_1 and φ_2 we obtain:

$$\dot{\psi}_1 = \dot{\theta}_1 + \alpha_1 \sin\theta_1 + \eta\alpha_1 \sin(\psi_2 - \psi_1 + \theta_1) - \eta\alpha_1 \sin(\psi_2 - \psi_1 + \theta_1 - \theta_2)$$

$$\dot{\psi}_2 = \dot{\theta}_2 + \eta\alpha_2 \sin\theta_2 + \alpha_2 \sin(\psi_1 - \psi_2 + \theta_2) - \alpha_2 \sin(\psi_1 - \psi_2 - \theta_1 + \theta_2) \tag{13}$$

An analysis of Eq. (13) shows that a complete decoupling is possible only if $\theta_1 = \theta_2 = 0$ which implies that the outputs $\dot{\varphi}_1$ and $\dot{\varphi}_2$ are zero which is of course unacceptable. We see then that any solution will involve a coupling of the two phase-locked loops, i. e., both $\dot{\varphi}_1$ and $\dot{\varphi}_2$ must be functions of ψ_1 and ψ_2 and we seek criteria which will minimize the influence of $\dot{\psi}_2$ and $\dot{\varphi}_1$ and $\dot{\psi}_1$ on $\dot{\varphi}_2$ (see Eq. (11)).

An acceptable solution is of course one in which θ_1 and θ_2 although not zero are very small. Under these conditions we can linearize Eq. (13) to obtain:

$$\dot{\psi}_1 = \dot{\theta}_1 + \alpha_1\theta_1 + n\alpha_1\theta_2 \cos(\psi_2 - \psi_1) \qquad 14(a)$$

$$\dot{\psi}_2 = \dot{\theta}_2 + n\alpha_2\theta_2 + \alpha_2\theta_1 \cos(\psi_2 - \psi_1) \qquad 14(b)$$

In deriving Eq. (14) we assumed $\sin\theta_1 \approx \theta_1$, $\sin\theta_2 \approx \theta_2$, $\cos\theta_1 \approx 1$, and $\cos\theta_2 \approx 1$. Eq. (14) represents two linear differential equations with time varying coefficients and $\dot{\psi}_1$ and $\dot{\psi}_2$ whose exact solutions are not easy to find analytically. We proceed by eliminating θ_2 to get a second order differential equation in θ_1.

Differentiating Eq. 14(a) yields:

$$\ddot{\psi}_1 = \ddot{\theta}_1 + \alpha_1\dot{\theta}_1 + n\alpha_1\dot{\theta}_2 \cos(\psi_2 - \psi_1) - n\alpha_1\theta_2(\dot{\psi}_2 - \dot{\psi}_1)\sin(\psi_2 - \psi_1)$$

replacing $\dot{\theta}_2$ from Eq. 14(b) above produces:

$$\ddot{\psi}_1 = \ddot{\theta}_1 + \alpha_1\dot{\theta}_1 + n\alpha_1 \cos(\psi_2 - \psi_1)\dot{\psi}_2 - n^2\alpha_1\alpha_2 \cos(\psi_2 - \psi_1)\theta_2 -$$

$$n\alpha_1\alpha_2 \cos^2(\psi_1 - \psi_2)\theta_1 - n\alpha_1(\dot{\psi}_2 - \dot{\psi}_1)\sin(\psi_2 - \psi_1)\theta_2$$

Rearranging and replacing θ_2 from 14(a) we obtain

$$\ddot{\theta}_1 + \dot{\theta}_1[\alpha_1 + n\alpha_2 + (\dot{\psi}_2 - \dot{\psi}_1)\tan(\psi_2 - \psi_1)] + \theta_1[n\alpha_1\alpha_2 \sin^2(\psi_2 - \psi_1) +$$

$$\alpha_1(\dot{\psi}_2 - \dot{\psi}_1)\tan(\psi_2 - \psi_1)] = \ddot{\psi}_1 - n\alpha_1\dot{\psi}_2 \cos(\psi_2 - \psi_1) + n\alpha_2\dot{\psi}_1 +$$

$$(\dot{\psi}_2 - \dot{\psi}_1)\dot{\psi}_1 \tan(\psi_2 - \psi_1) \qquad (15)$$

We note that the poles of Eq. (15) will vary with time on the real axis and it can readily be shown that they will wander into the right half plane for

$$n\alpha_2 < |(\dot{\psi}_2 - \dot{\psi}_1)\tan(\psi_2 - \psi_1)| \qquad (16)$$

If we had rearranged terms in Eq. (14) and solved for θ_2 instead of θ_1 we would have the conditions that poles will lie in the right half plane when

$$\alpha_1 < |(\dot{\psi}_2 - \dot{\psi}_1)\tan(\psi_2 - \psi_1)| \tag{17}$$

In such a case our assumption that θ_1 be small will not be valid and the solution will be accompanied by large oscillations which can easily bring the system in and out of lock.

As a first example let us assume the case of a CW interferer with no frequency offset, i. e., $\psi_1 = 0$ and a sinusoidally frequency modulated desired signal, i. e., $\psi_2 = \beta \cos \omega_m t$. We further specialize to the case of small β, i. e., $\beta \ll \pi/2$. For stability we require

$$\eta\alpha_2 > \left| \frac{\beta^2\omega_m}{2} \sin 2\omega t \right| = \frac{\beta^2\omega_m}{2}$$

and

$$\alpha_1 > \frac{\beta^2\omega_m}{2}$$

i. e., the hold-in-range of both phase-lock loops should be larger than the largest frequency deviation between the two received signals. Under these conditions θ_1 of Eq. (15) will be an oscillatory function whose fundamental frequency is ω_m and whose amplitude can be shown to be approximately given by

$$|\theta_1| = \frac{4\eta\alpha_1\beta\sqrt{\omega_m^2[(4 + 3\eta\alpha_1\alpha_2(\beta/\omega_m)^2]^2 + 16(\alpha_1 + \eta\alpha_2)^2}}{16(\alpha_1 + \eta\alpha_2)^2 - \omega_m^2[3(\eta\alpha_1\alpha_2(\beta/\omega_m)^2)^2 - 8\eta\alpha_1\alpha_2(\beta/\omega_m)^2 - 16]} \tag{18}$$

A computer aided analysis of Eq. (15) for a number of other types of interferers and desired signals is in preparation and will be reported shortly with more quantitative criteria of design.

Another example which provides insight into system stability is the following. Essentially we strive for a design which yields $\dot{\theta}_1 = \dot{\theta}_2 = 0$ (see Eq. 12). This implies θ_1 and θ_2 are constants. Substituting the condition $\dot{\theta}_1 = \dot{\theta}_2 = 0$ into Eq. (13) and defining $\dot{\psi} \equiv \dot{\psi}_1 - \dot{\psi}_2$ we obtain:

$$\dot{\psi} = \alpha_1 \sin\theta_1 - \eta\alpha_2 \sin\theta_2 + \eta\alpha_1 \sin(\theta_1 - \psi) -$$

$$\eta\alpha_1 \sin(\theta_1 - \theta_2 - \psi) - \alpha_2 \sin(\psi + \theta_2) + \alpha_2 \sin(\psi - \theta_1 + \theta_2) \tag{19}$$

If for a given ψ this equality is satisfied we have such a solution.

As an example let us assume a frequency offset between the two received carriers $\dot{\psi} = \Delta\omega$. Then such a solution will exist if the following equations are satisfied simultaneously.

$$\Delta\omega = \alpha_1 \sin\theta_1 - \eta\alpha_2 \sin\theta_2 \tag{20}$$

$$\eta\alpha_1 \sin\theta_1 - \eta\alpha_1 \sin(\theta_1 - \theta_2) - \alpha_2 \sin\theta_2 + \alpha_2 \sin(\theta_2 - \theta_1) = 0 \tag{21}$$

$$-\eta\alpha_1 \cos\theta_1 + \eta\alpha_1 \cos(\theta_1 - \theta_2) - \alpha_2 \cos\theta_2 + \alpha_2 \cos(\theta_2 - \theta_1) = 0 \tag{22}$$

which yields the upper bound condition on the frequency offset

$$\Delta\omega < \alpha_1 + \eta\alpha_2 .$$

A simple solution when θ_1 and θ_2 are small can readily be found in this example by using $\sin\theta_1 \approx \theta_1$, $\sin\theta_2 \approx \theta_2$, $\cos\theta_2 \approx 1$, and $\cos\theta_1 \approx 1$.

For this restriction we have

$$\alpha_1\theta_1 - \eta\alpha_2\theta_2 = \Delta\omega \tag{23}$$

$$-\alpha_2\theta_1 + \eta\alpha_1\theta_2 = 0 \tag{24}$$

which, when solved simultaneously, yields

$$\theta_1 = \frac{\alpha_1 \Delta\omega}{(\alpha_1^2 - \alpha_2^2)} \tag{25}$$

and

$$\theta_2 = \frac{\alpha_2 \Delta\omega}{\eta(\alpha_1^2 - \alpha_2^2)} \tag{26}$$

which is valid to within 10% if $|\theta_1|$ and $|\theta_2|$ are each less than 0.4 radians. Given a fixed loop design (α_1, α_2), Eq. (25) and Eq. (26) yield the maximum displacement of received carrier frequencies.

Additional analytical studies investigating theoretical models for higher order loops and determining criteria for stable design are now in progress.

VI. A Uniform Power Spectral Density Jamming Signal

It is often useful in electronic countermeasures to transmit high power noise over some prescribed band of frequencies in an attempt to interfere with transmissions from an unfriendly source. Since we do not know with any certitude the frequencies at which the source transmits and/or receives, it is desirable to use a high power signal with a continuous uniform power spectral density bandlimited over some frequency band for the noise jammer. In this work a technique is described for generating such a signal with flexibility in designing for its center frequency and bandwidth.

The technique employed utilizes Woodward's Theorem [11] which states that the spectrum of an FM signal with large modulation index (β) takes on the same shape as the probability density function (pdf) of the amplitude of the modulating waveform. As a practical rule of thumb, the rms modulation index, β_{rms}, defined as the ratio of the rms frequency deviation of the FM modulator's output to the rms frequency of the input modulating waveform should exceed 10 for Woodward's Theorem to be valid. Blackman and McAlpine [11] have shown, however, that for the special case of a gaussian modulating signal, β_{rms} can be as low as one and reasonably good agreement between the output spectrum and the pdf of the input modulating waveform is still achieved.

A block diagram of the system used to generate the noise jammer is shown in Fig.23. As can be seen, a nonlinear network is used to transform gaussian noise into a stochastic signal whose amplitude has a uniform pdf. The resultant signal is then used to frequency modulate a carrier with large β. The spectrum of the transmitted signal will then be uniform and continuous centered around the carrier frequency with bandwidth (BW) approximately equal to twice the peak frequency deviation (Carson's Rule). The power contained in the transmitted signal can be made large by using a high power FM modulator or by using efficient nonlinear RF power amplifiers following the modulator.

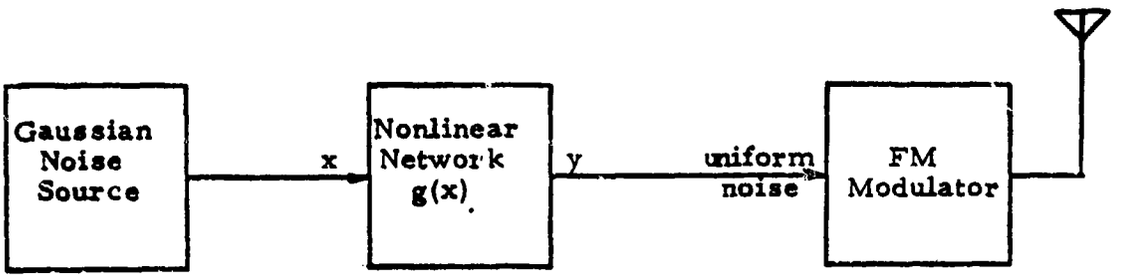

Fig. 23 Generation of a uniform power spectral density jamming signal.

Nonlinear Network

The nonlinear network required in Fig. 23 is readily determined using the techniques relating to transformation of a random variable. If x (see Fig.23)is assumed to be a zero mean stationary gaussian random process with variance σ_x^2, and we desire y to be a zero mean uniformly distributed process over the normalized interval $[-\frac{1}{2}, \frac{1}{2}]$, then the transfer function of the nonlinear network can be shown to take on the form[12]

$$g(x) = \text{Erf}\left(\frac{x}{\sigma_x}\right) - \frac{1}{2} \tag{27}$$

where the error function,

$$\text{Erf}\left(\frac{x}{\sigma_x}\right) = \frac{1}{\sqrt{2\pi}} \int_{-\infty}^{x/\sigma_x} e^{-z^2/2}\, dz \tag{28}$$

is well tabulated.[13]

In the laboratory a commercially available gaussian noise generator (GR1382) and an FM modulator (Wavetek 184) were used to implement the system described in Fig.23. Although a broadband nonlinear diode wave-shaping network could be designed with transfer function proportional to $\text{Erf}(x/\sigma_x)$, for simplicity the constant current biased bipolar junction transistor differential pair configuration shown in Fig.24 was employed.

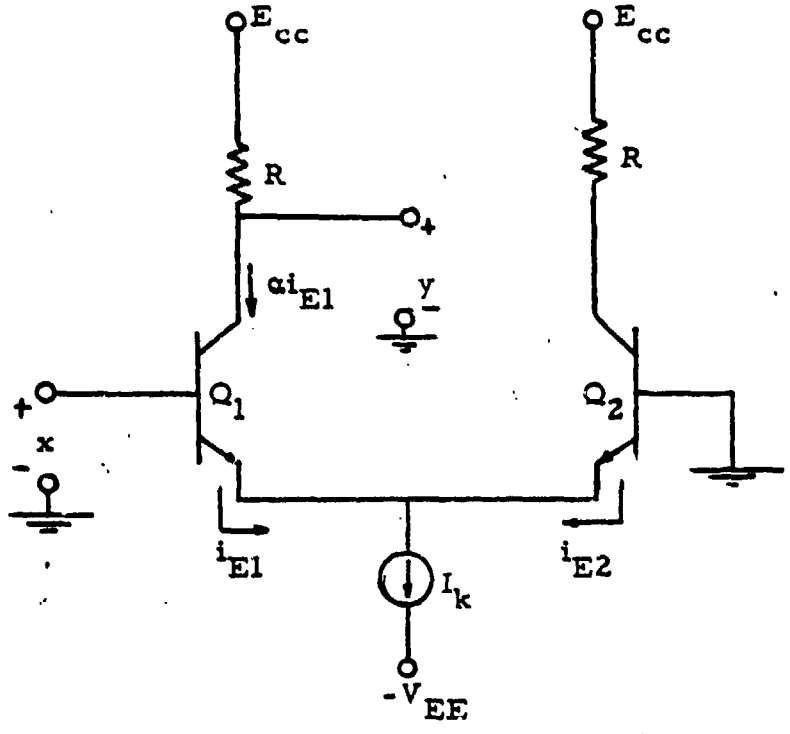

Fig. 24 Constant current biased bipolar junction transistor differential pair configuration.

The transfer characteristic relating the output voltage y and the applied input signal x is given by[14]

$$y = E_{cc} - \frac{\alpha I_k R}{2}\left[1 + \tanh\left(\frac{qx}{2kT}\right)\right] \qquad (29)$$

where $\frac{kT}{q}$ = 26mV at room temperature (T = 300°K) and α denotes the transistor "alpha". The shape of this characteristic is governed by the term $\frac{1}{2}\left[1 + \tanh\left(\frac{x}{52mV}\right)\right]$. The remaining terms in Eq.(29) determine the magnitude (peak-to-peak swing) and dc level of the differential pair output voltage. This transfer function has the same general form as the desired error function characteristic as illustrated in Fig.25. Both agree at x = 0, x = ∞, and at x = -∞. To determine that value of σ_x which provides for a reasonable "match-up" of the two transfer functions over other values of x, we equate $\mathrm{Erf}\left(\frac{x}{\sigma_x}\right)$ to $\frac{1}{2}\left[1 + \tanh\left(\frac{x}{52mV}\right)\right]$ at points a and b on Fig.25. Carrying out this match-up

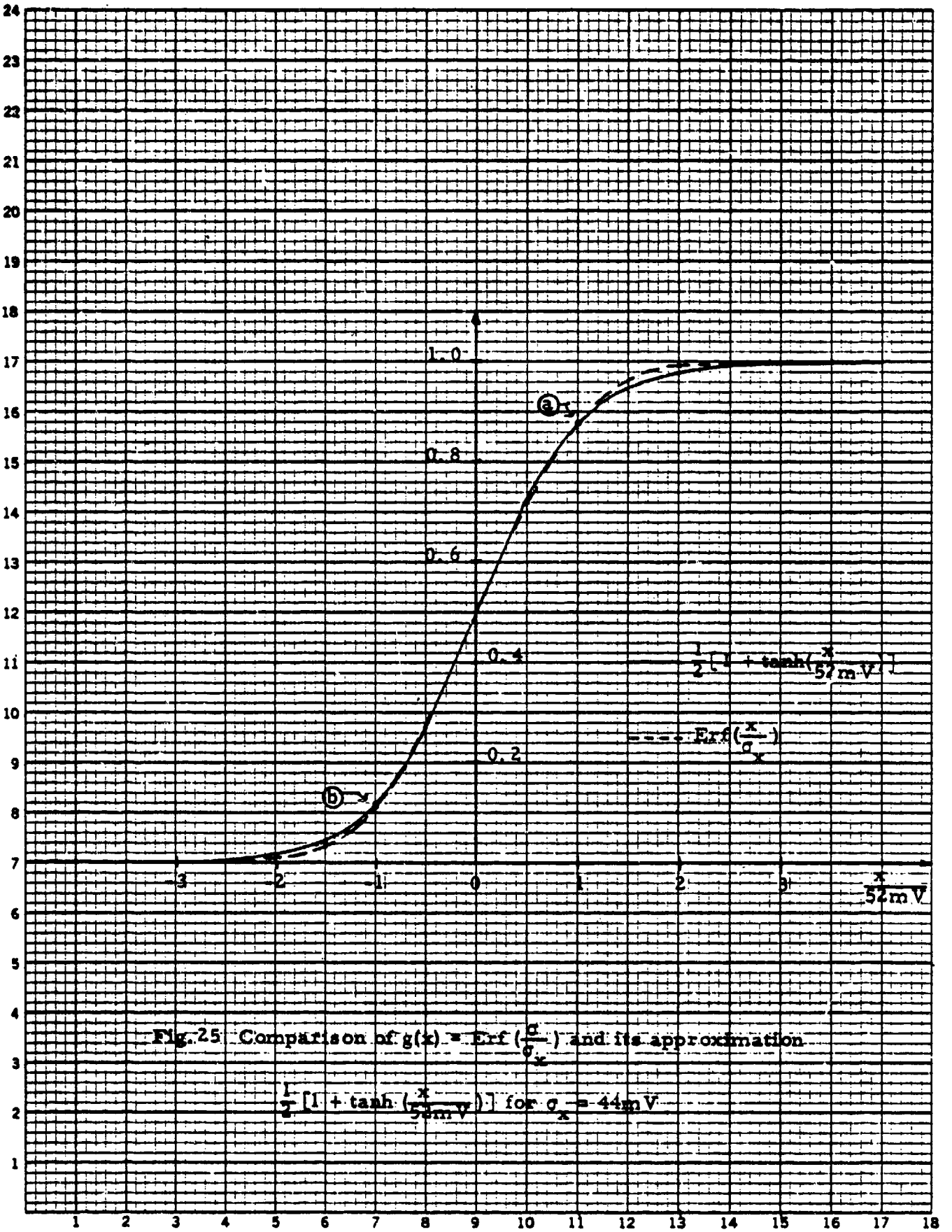

Fig. 25 Comparison of $g(x) = Erf(\frac{x}{\sigma_x})$ and its approximation $\frac{1}{2}[1 + \tanh(\frac{x}{52mV})]$ for $\sigma_x = 44mV$

process σ_x is found to be 44mV. For this value the mean square error between the $Erf(x/\sigma_x)$ and its approximating curve is only 2.35% over the range $-4 \leq x \leq 4$. Although the location of points a and b on Fig. 25 may seem somewhat arbitrary, the reader can readily show that the numerical value of σ_x is not very sensitive to that choice of location.

The differential pair dc output voltage, $E_{cc} - \alpha I_k R/2$ will shift the carrier frequency of the FM modulator. If desired, it can be eliminated by inserting a dc level shifter or coupling capacitor between the nonlinear network and FM modulator of Fig. 23, or it may be used as a control to adjust the center frequency of the jammer signal generated by the FM modulator.

Experimental Results

The block diagram of the total experimental set-up used is shown in Fig.26. The pdf machine was Polytechnic built and is described in Ref. (15). To insure proper operation of the pdf machine, density measurements were initially made with sinusoids, triangle waves, and square waves and compared with known theoretical responses. The pdf of the GR noise generator was then checked to insure it was gaussian and zero mean. The four pole maximally flat design Krohn-Hite variable low pass filter following the gaussian noise generator permits control of the rms modulation index of the FM modulator output.

Since the circuit of Fig.24 requires well matched transistors, the LM3086 integrated circuit transistor array designed for such configurations was used for the nonlinear network. To insure its proper operation the static transfer characteristic was measured. Excellent agreement with the normalized response shown in Fig.25 was obtained. Typical responses of the pdf of the nonlinear circuit output and the corresponding oscillogram of the output spectrum are shown in Fig.27a and 27b. The pdf is uniform as expected, and the output signal has a uniform power spectral density, as Woodward's Theorem predicts. The experimental result of Fig.27b reveals that the spectrum is centered around the carrier frequency of 200kHz, the free running frequency of the FM generator, with a bandwidth of 237kHz. Theoretically, the bandwidth expected is twice the peak frequency deviation which is given by the peak-to-peak

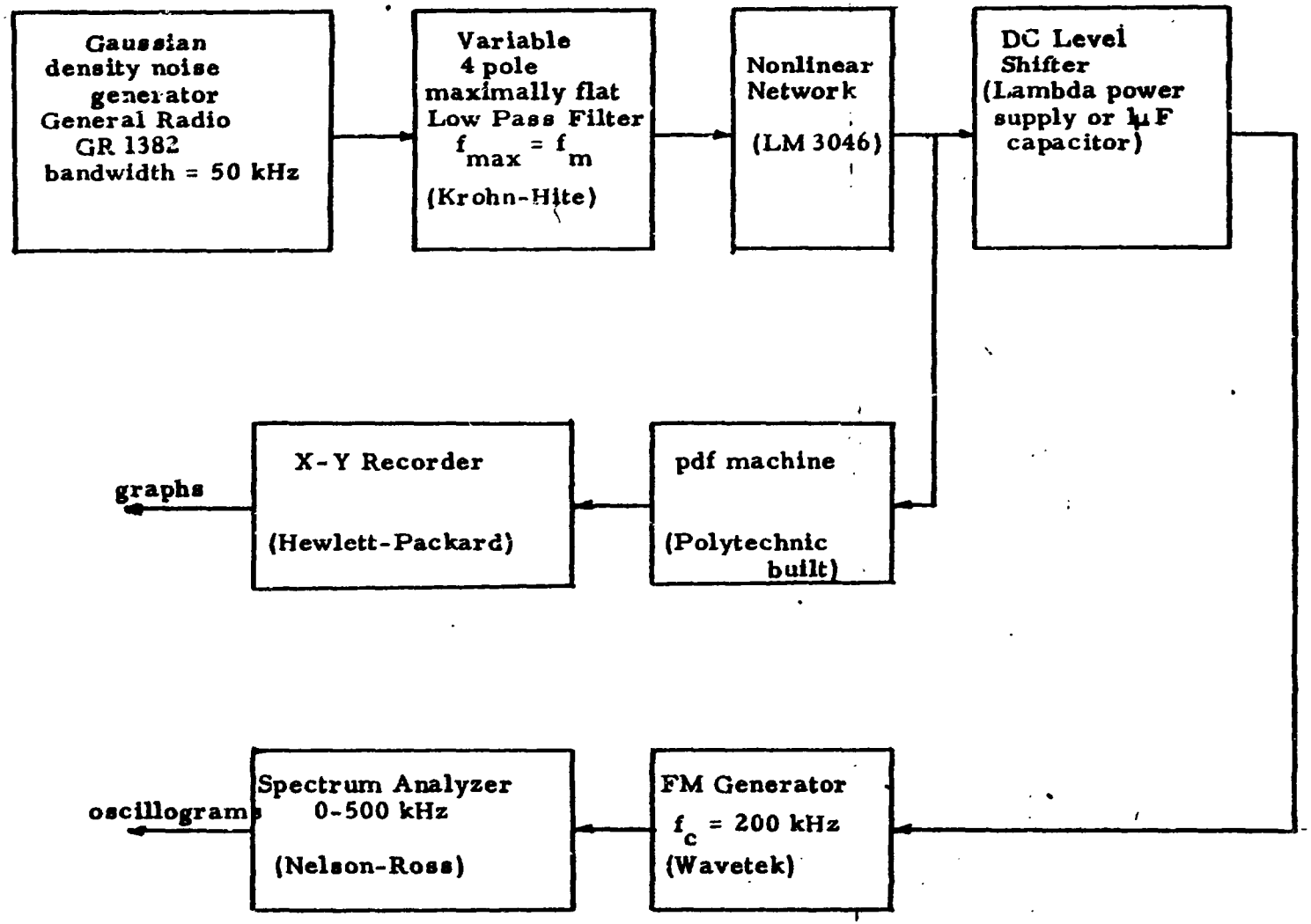

Fig. 26 Block diagram of experimental set-up.

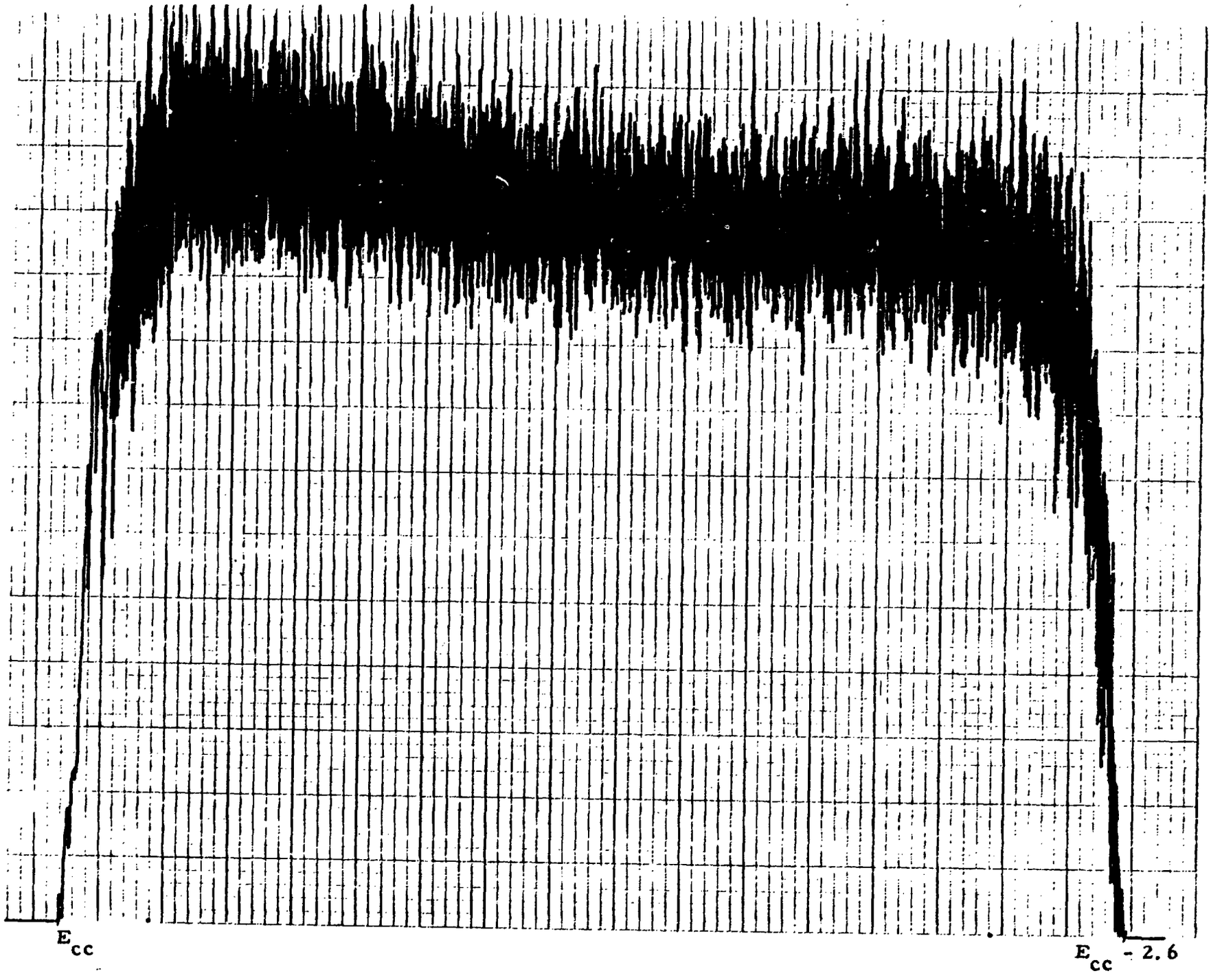

Fig. 27a pdf of nonlinear differential pair output with gaussian

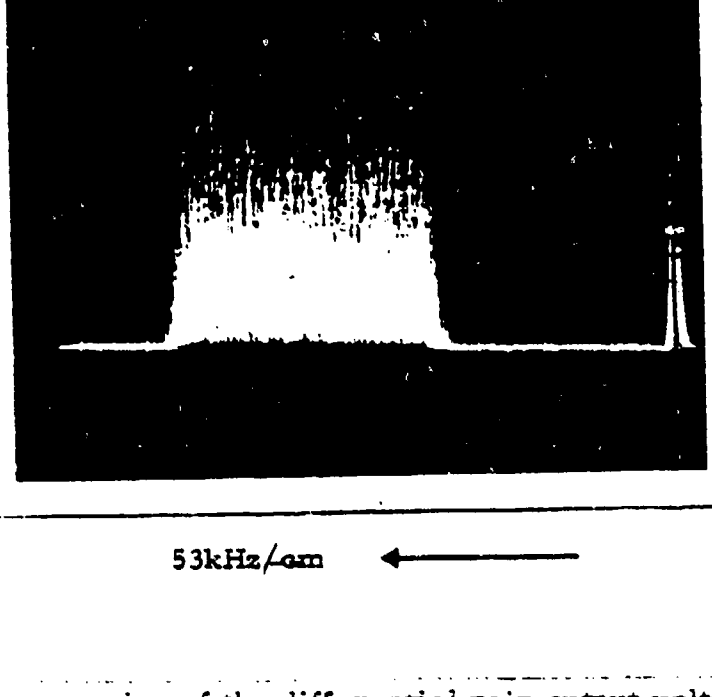

Fig. 27b FM modulator output spectrum (center frequency = 200kHz; bandwidth = 237 kHz; β_{rms} = 29.6, sweep speed = 5 sec/cm; impulse at right of the oscillogram denotes dc).

swing of the differential pair output voltage ($I_k R$) multiplied by the FM modulator's sensitivity K_g(kHz/volt). Using the experimental values I_k = 1.37mA, R = 2K ohm, K_g = 100kHz/volt yields a theoretical BW of 274kHz. The 14% discrepancy from the measured value can easily be accounted for by component and measurement tolerances and Carson's Rule approximations. Increasing the value of R or I_k of Fig. 2 will increase the peak-to-peak swing at the differential pair output, and hence increase the rms voltage at the FM modulator input and, subsequently, the bandwidth of the modulator's output spectrum. This was verified experimentally in a quantitative manner as the numerical example just presented. This feature provides a useful mechanism for electronically or manually controlling BW. In addition to varying the parameters R and I_k, the FM modulation index was varied over the range $10 \leq \beta_{rms} \leq 50$ by adjusting the bandwidth (f_m) of the Krohn-Hite low pass filter of Fig. 26. Rectangular output spectrums with Carson's Rule bandwidths were experimentally obtained throughout this range.

VII. Technological Applications

The demodulator possesses a number of important technological applications. Among these include:

(1) electronic warfare applications as an anti-jamming receiver to combat intentional interferers whether stronger or weaker than the desired signal.

(2) electronic countermeasures: one could intentionally corrupt a frequency modulated carrier with a stronger interferer. A conventional receiver would by the "capture effect" demodulate the stronger FM carrier (perhaps modulated by a decoy message) while the novel detector could easily be designed to detect the desired weaker FM carrier.

(3) as a communications receiver for analog or digital FM signals to suppress the degradation in detected output signal-to-noise ratio due to the presence of co-channel or adjacent channel interferers.

(4) provide for "spectrum sharing" to relieve the ever increasing crowding in the radio frequency spectrum.

(5) suppress the effects of multipath interference including ghosts in TV reception.

(6) supplement the techniques of steerable antenna nulling which fail (a) when the received carrier amplitude ratio, η, is near unity, and (b) when the source of interference comes from the same direction (or mirror direction) as the desired signal.

The physical insight obtained in this study on the acquisition behavior of the novel demodulator will undoubtedly be useful in examining many of the aforementioned applications in future research efforts.

VIII. Future Research Objectives

Although numerous results have already been obtained, a number of basic research problems still remain unsolved. They are not simple extensions of previous work performed but rather represent new and important ideas yet to be explored.

A. The research sponsored on ARO Grant DAAG 29-77-G-0232 has led to improved techniques for enabling the cross coupled PLL receiver structure to suppress numerous types of interferers. Fig. 28 describes a block diagram of such a new system. This detector cross correlates the in-phase and quadrature phase components of the PLL voltage controlled oscillator (VCO) output signals with the PLL inputs to provide for an adaptive feedback closed loop system for estimating both the instantaneous phase and amplitude of two received co-channel signals. It is expected such a scheme will experience significant improvement over the performance capabilities of the cross coupled PLL receiver of Fig. 9 which utilizes an open loop control for estimating the instantaneous amplitude of the received signals.

We propose to undertake an analytical and experimental study of this new demodulator. The system can be theoretically modeled by six coupled nonlinear differential equations. Among our objectives include:

(1) Theoretically examine the transient acquisition behavior for the demodulator described on the attached block diagram using computer aided analysis of the system's defining equations. From such a study we expect to (a) determine the range of loop parameters over which successful acquisition, separation, and detection of the received co-channel signals can be achieved, and (b) determine that set of loop parameters which is relatively independent, i. e., robust with respect to input signal conditions. Such a design would be useful in suppressing a variety of interferers without the need to switch loop parameters. Among the interferers to be included in the analytical study include CW, CW with frequency offset, wideband FM, narrowband FM, AM, AM/FM, pulsed RF, and noise jammers.

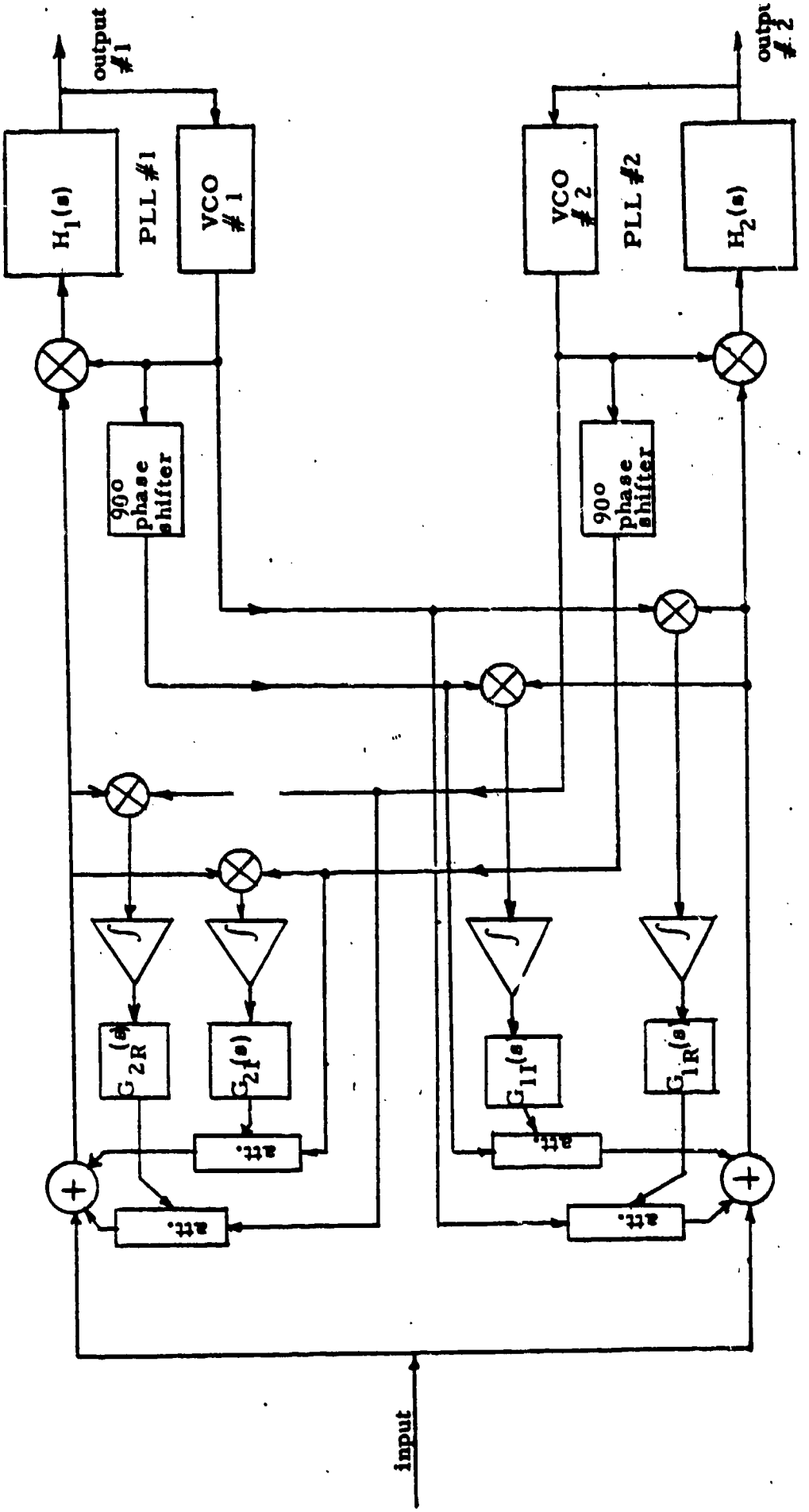

Fig. 28 Cross Coupled PLL Receiver with Adaptive Closed Loop Feedback Control

(2) Repeat objective (1) above for the case when limiters are inserted at each PLL input and make comparisons with the results obtained above without limiters.

(3) Using computer aided analysis determine the effect of noise on the acquisition performance of the cross coupled PLL structure when driven by a desired FM signal corrupted by a co-channel interferer plus narrowband gaussian noise.

(4) Theoretically examine the stability of the system by developing phase plane portraits for each PLL and determine locations of any possible unstable operating points and/or conditions which may generate limit cycles.

(5) Design and construct experimental models to investigate the practical performance capabilities and limitations of this new system in suppressing numerous types of interferers.

B. Studies [18] based on information theory have set upper bounds for the detected output signal to noise ratio (SNR) performance of analog FM communication systems. None of the conventional FM receivers (limiter-discriminators) come close to approximating that bound. It is proposed here to treat the demodulator's received noise signal as the co-channel interferer (or include it with the interferer if one is present) and examine the capabilities and limitations of the cross coupled PLL demodulator in suppressing the effects of the noise on the desired signal. One of the specific objectives will be to determine how close the detected desired output SNR comes to the predicted theoretical upper bound established by information theory. Another is to determine the capabilities and limitations of the cross coupled PLL in suppressing narrowband gaussian noise jammers. This represents another new and exciting basic research problem not previously investigated under this program.

C. Another objective of the proposed research is to theoretically and experimentally determine the capabilities and limitations of the novel detector in suppressing the degradation of receiver performance due to multipath. Both specular and diffuse multipath cases will be considered. Multipath interferers have characteristics significantly different and unique from other interferers. Here the echo is not independent from the desired signal but rather correlated to the dominant path transmission.

A simple two-ray model for specular multipath is illustrated in Fig. 29. In this simplified model the receiver sees the direct path transmission $s_d(t)$ plus a reflection $\eta\, s_d(t-\tau)$ where η is a scalar constant and τ_m denotes the relative time delay between the direct path transmission and the multipath "echo".

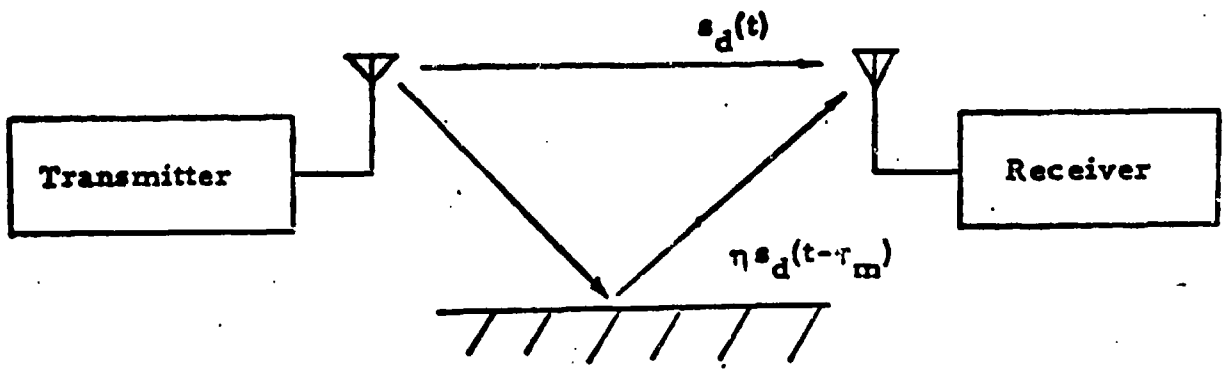

Fig. 29 Multipath Channel Model

The multipath reflection behaves as a co-channel interferer since the echo occupies the same frequency band as the desired path signal. In an FM communication system $s_d(t)$ and $\eta s_d(t-\tau_m)$ take the form

$$s_d(t) = A \cos[\omega_o t + \phi(t)]$$

$$\eta s_d(t-\tau_m) = \eta A \cos[\omega_o(t-\tau_m) + \phi(t-\tau_m)]$$

where A denotes the carrier amplitude, ω_o the carrier frequency, and $\dot{\phi}(t)$ the information signal bandlimited to f_m which frequency modulates the carrier. If τ_m is small then the interferer is highly correlated to the desired signal. Conversely, if τ_m is large, the multipath echo appears as an uncorrelated interferer.

The effect of the correlation between the desired direct path transmission and the reflected multipath interferer on the performance of the demodulator will be determined.

The output SNR versus the received CNR will be evaluated for the novel detector above and below its FM threshold level when detecting analog FM signals in a multipath plus narrowband gaussian noise environment for several values of η, several FM modulation indices, and different modulation signals. Probability of making decision errors versus CNR will be determined for the novel detector when demodulating binary FSK signals corrupted by multipath interferers plus noise.

Wherever appropriate, all results obtained on the novel detector will be compared to other receiver structures discussed in the literature.

Ghosts in TV receivers are just one example of multipath interferers. Since the cross coupled PLL detector can in theory be designed to accommodate AM received signals (see Fig. 9), it has potential in suppressing ghosts in TV reception. At this time its capabilities and limitations in this area are unknown and remain as a topic of future research.

D. The capture effect of a phase-locked loop will be theoretically and experimentally examined. Much work has been reported [16-17] on the capture effect of FM discriminators such as the pulse count detectors, Foster-Seely discriminators, and Ratio detectors. All studies conclude that the finite capture effect exhibited by such FM demodulators is due to their finite bandwidth. No corresponding studies have been performed for tracking demodulators such as the PLL. The capture phenomenon plays a major role in the operation of the cross-coupled PLL receiver and hence understanding how to design a PLL to enhance its capture effect is fundamental to the overall design of the cross-coupled PLL receiver.

E. Physical insight obtained from the theoretical and experimental study of the cross-coupled PLL receiver will undoubtedly lead to alternate receiver structures with potential for improved performance. One such structure is shown in Figure 30.

Such a scheme is useful when the initial frequency difference between the VCO free running rest frequency and PLL input is large. In such cases the discriminator provides the necessary dc control voltage to pull the VCO toward the direction of lock. After lock is achieved, the narrowband PLL will provide a good estimate of the instantaneous phase of its input signal.

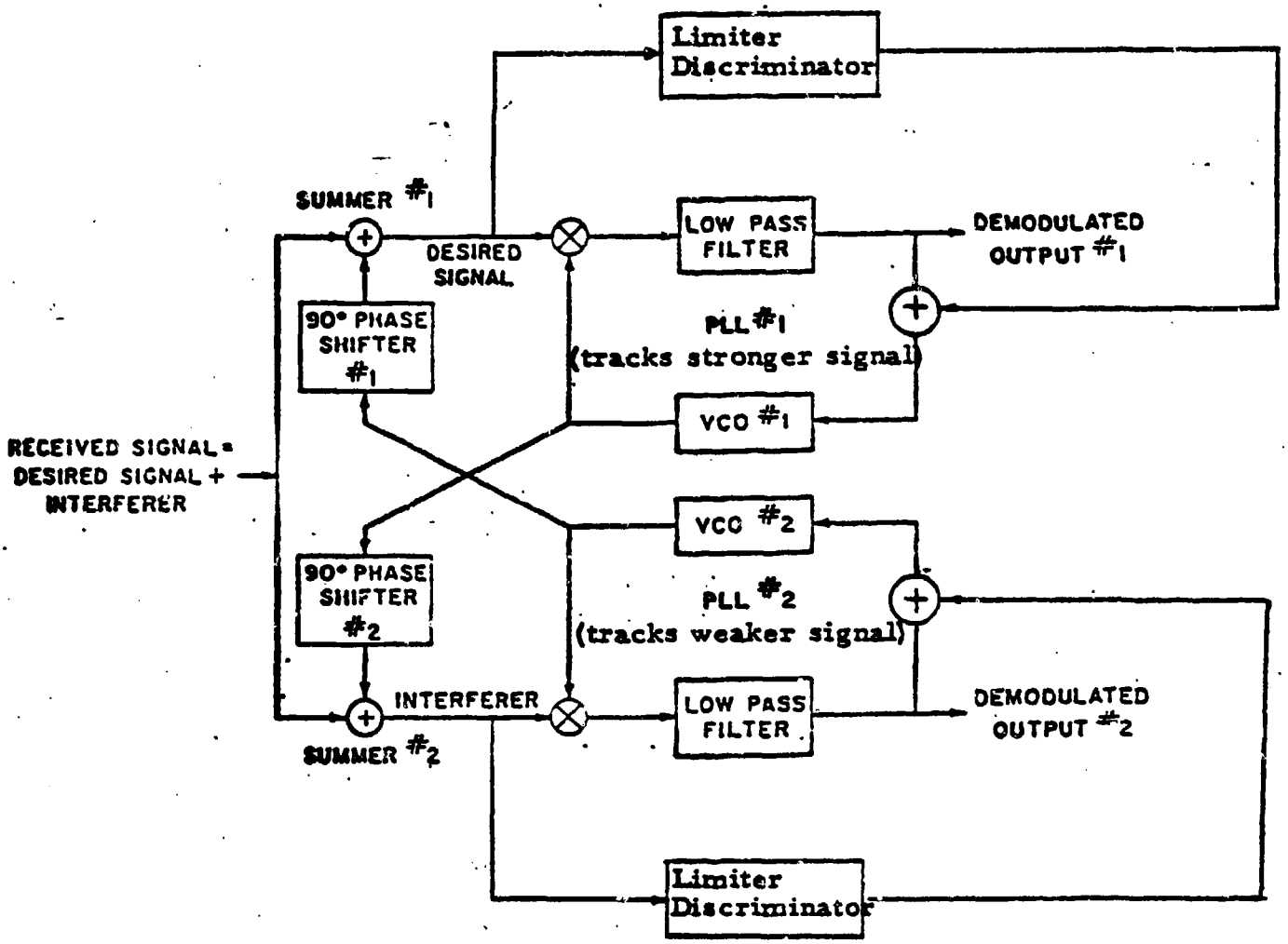

Fig.30 Improved acquisition for the cross coupled PLL receiver

F. Theoretically determine the acquisition or "pull-in" time for the cross-coupled PLL receiver to acquire lock, successfully cancel the interferer, and demodulate the desired received signal. Rapid acquisition is particularly important in high speed digital FM communication links and fast frequency hopping spread spectrum communication systems. Loop parameters which simultaneously provide for rapid acquisition and good interference and noise suppression parameters will be sought. This work should not be confused with the stability regions already obtained from studying the acquisition behavior of the receiver. The time it takes to acquire lock is a new problem to be solved and not a simple extension of work already performed.

G. Experimentally examine adaptive designs which utilize wideband first order phase-locked loops during the initial lock-up transient interval for rapid acquisition, and then, after lock is achieved, are electronically switched to narrowband second order tracking loops for good signal-to-noise ratio performance.

H. Theoretically and experimentally examine the behavior of the cross coupled PLL receiver with limiters preceding each PLL as shown in Fig.31. As can be seen from Fig.15a small values of η require PLL #2 to be designed with large dc loop gain, i.e., large α_2 in order to insure successful separation and demodulation of the two received co-channel signals. This seems plausible since the hold-in-range of PLL #2 is proportional to $\eta\alpha_2$. The curves shown in Fig. 15a approximately coalesce into one curve if the vertical axis is changed from α_2 to $\eta\alpha_2$. In most

applications η is unknown and in some cases a function of time. To insure successful separation of the interferer and demodulation of the desired signal, a worse case design $\alpha_2 \gg \alpha_1$ would be required. Such wideband phase-locked loops may lead to impractical designs and/or designs which are vulnerable to noise which is always present in the received signal. Limiters preceding each PLL can overcome this problem by providing a constant amplitude signal to each PLL so that even if η is small, PLL #2's bandwidth need not be designed large. This new receiver structure is described by a new system of coupled nonlinear differential equations to take into account the addition of two nonlinear networks - namely the limiters. New computer aided solutions are required for this research problem.

L. Conceive and examine alternate designs for experimental models operating in the 10-100MHz frequency range which possess the capability of increasing the depth of the cancellation null so that the detector can suppress co-channel CW, AM, FM, AM/FM, or noise jammer interferers which are as much as 40dB stronger than the desired signal.

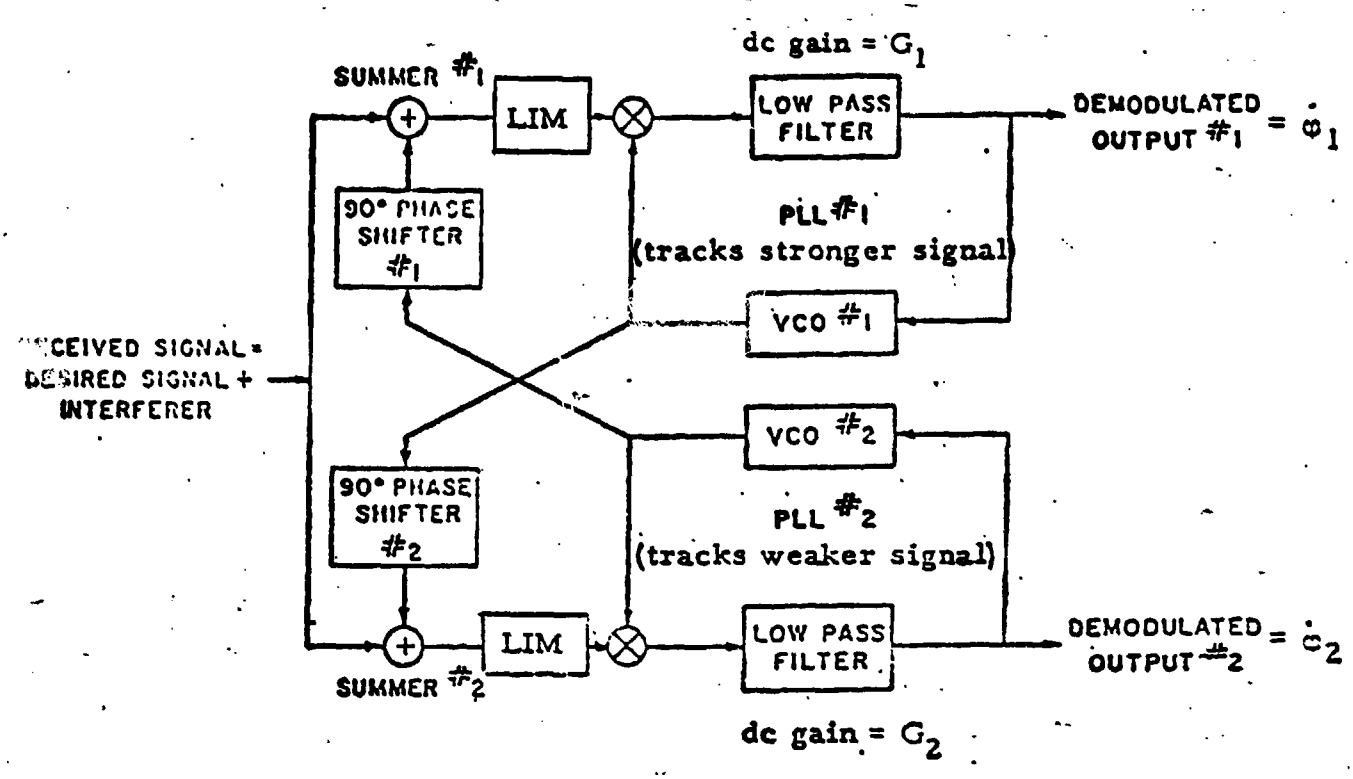

Figure 31 Cross-coupled PLL Receiver with Limiters

IX. Scientific Personnel

A. ARO Supported

1. Professor F. A. Cassara, principal investigator - directed the research effort in both theoretical and experimental phases; performed analytical studies related to the transient acquisition behavior of the cross coupled PLL demodulator; conceived signal design of the uniform power spectral density jamming signal.

2. Professor H. Schachter - directed effort relating to theoretical derivation of the maximum a posteriori estimator for suppressing interchannel interference in FM along with the computer simulation study and interpretation of the results. Also responsible for section on theoretical models.

B. Unsupported

1. Tippure S. Sundresh, Ph. D. graduate student - responsible for the analytical derivation of the maximum a posteriori estimator for suppressing interchannel interference in FM.

2. Gerald Simowitz, Ph. D. graduate student - assisted in design, construction, and experimental analysis of the cross-coupled PLL demodulator.

3. Edwin Muth - undergraduate student - responsible for experimental results relating to the design of a uniform power spectral density jamming signal.

4. Dale Gettys - undergraduate student - same contribution as E. Muth.

X. Publications on the Cross-Coupled PLL Receiver

1. F. A. Cassara, T. S. Sundresh, and H. Schachter, "Suppression of Interchannel Interference in FM Receivers," Digest of Papers, IEEE Canadian Conference on Communications and Power, Montreal, Canada, pp. 63-65, October 1976.

2. T. S. Sundresh, F. A. Cassara, and H. Schachter, "A Novel FM Detector for Suppression of Interchannel Interference in FM Receivers," Conference Proceedings Sixth European Microwave Conference, pp. 460-463, September 1976.

3. T. S. Sundresh, F. A. Cassara, and H. Schachter, "Maximum A Posteriori Estimator for Suppression of Interchannel Interference in FM Receivers," IEEE Transactions on Communications, Vol. 25, No. 12, December 1977, pp. 1480-1485.

*4. F. A. Cassara, E. Muth, and D. Gettys, "A Uniform Power Spectral Density Jamming Signal," Proc. of the IEEE, February 1979, pp. 330-332.

*5. F. A. Cassara and H. Schachter, "Transient Acquisition Behavior of the Cross Coupled Phase Locked Loop FM Demodulator," to be submitted to IEEE Trans. on Communications and is currently in the review process.

*6. F. A. Cassara, H. Schachter, and G. Simowitz, "Cross Coupled Phase-Locked Loop FM Demodulator, "Proceedings of 22nd Midwest Symposium on Circuits and Systems, June 17-19, 1979, pp. 475-481.

* Supported by ARO Grant DAAG 29-77-G-0232.

BIBLIOGRAPHY

1. T. S. Sundresh, "Interchannel Interference in FM Receivers," Ph. D. Dissertation, Polytechnic Institute of Brooklyn, Brooklyn, New York, June 1972.

2. O. Shimbo and R. Fang, "Effects of Co-Channel Interference and Gaussian Noise in M-ary PSK Systems," Comsat Technical Review, Vol. 3, No. 1, pp. 183-206, Spring 1973.

3. L. Wang, "Error Probability of a Binary Noncoherent FSK System in the Presence of Two CW Tone Interferers," IEEE Trans. on Communications, Vol. 22, No. 12, pp. 1948-1949, Dec. 1974.

4. R. E. Ziemer and W. H. Tranter, Principles of Communications, Houghton Mifflin Co., Boston, Mass., pp. 346-356, 1976.

5. J. M. Gutwein and R. G. Bland, "Aeronautical L-Band Technology Tests with the ATS-6 Satellite," 1976 IEEE Canadian Communications and Power Conference Digest, pp. 106-108.

6. H. C. Salven and C. B. Duncombe, "Aircraft-Satellite Channels; Modern Evaluation," IEEE Trans. on Comm., July 1975, pp. 690-705.

7. P. F. Panter, Modulation, Noise, and Spectral Analysis, McGraw-Hill, New York, New York, 1965, pp. 363-370.

8. H. L. Van Trees, "Detection, Estimation and Modulation Theory," John Wiley and Sons, Inc., New York, 1968.

9. Mischa Schwartz, "Abstract Vector Spaces Applied to Problems in Detection and Estimation Theory," Trans. IEEE on Information Theory, pp. 327-336, July 1966.

10. S. O. Rice, "Noise in FM Receivers," Time Series Analysis, M. Rosenblatt, Ed., New York: Wiley, 1963, Chapter 25.

11. Nelson Blachman and George McAlpine, "The Spectrum of a High-Index FM Waveform: Woodward's Theorem Revisited," IEEE Transactions on Communication Technology, Vol. 17, No. 2, April 1969, pp. 201-207.

12. A. Papoulis, Probability, Random Variables, and Stochastic Processes, McGraw-Hill, 1965, Chapter 5.

13. Paul Meyer, Introductory Probability and Statistical Applications, Addison-Wesley, 1970, pp. 342-343.

14. K. K. Clarke and D. T. Hess, Communication Circuits: Analysis and Design, Addison-Wesley, 1971, pp. 114-115.

15. K. K. Clarke, "Electronic Probability Density Machine," IEEE Transactions on Instrumentation and Measurement, June 1966, pp. 25-29.

16. I. Bruyland, "The Influence of Finite Bandwidth on the Capture Effect in FM Demodulators," IEEE Trans. on Comm., Vol. 26, No. 6, June 1978, pp. 776-784.

17. K. Leentvaar and J. H. Flint, "The Capture Effect in FM Receivers," IEEE Trans. on Comm., Vol. 24, May 1976, pp. 531-539.

18. T. Goblick, "Theoretical Limitations on the Transmission of Data from Analog Sources," IEEE Trans. on Information Theory, Vol. 11, No. 4, October 1965, pp. 558-567.

Appendix A

The derivation of Eq. (7) follows from an evaluation of the two parts of Eq. (6). The first part is

$$\frac{\partial}{\partial x_1} \log p(v|x_1) = \frac{1}{p(v|x_1)} \cdot \frac{\partial}{\partial x_1} \int_{-\infty}^{\infty} p(v|x_1, x_2) p(x_2)\, dx_2$$

$$= \frac{1}{p(v|x_1)} \frac{\partial}{\partial x_1} \int_{-\infty}^{\infty} p(x_2)\, k_1 \exp\left\{-\frac{1}{2}\left((v-s_1-s_2), R_n^{-1}(v-s_1-s_2)\right)\right\} dx_2 \tag{A1}$$

where k_1 is a constant and (a, b) denctes inner product of a and b given by

$$(a, b) = \int_0^T a(t)\, b(t)\, dt .$$

The operator R_n^{-1} in Eq(A1) is defined by[9]

$$R_n^{-1}(v-s_1-s_2) = \int_0^T R_n^{-1}(t,u)\left[v(u)-s_1(u)-s_2(u)\right] du \tag{A2}$$

or equivalently,

$$v-s_1-s_2 = \int_0^T R_n(t,u)\left[R_n^{-1}(v(\mu)-s_1(\mu)-s_2(\mu)\right] du$$

For white additive noise, $R_n(t,\mu) = \delta(t-u)$ so that

$$R_n^{-1}[v-s_1-s_2] = v-s_1-s_2 \tag{A3}$$

Substituting Eq. (A3) into Eq. (A1) and carrying out the indicated differentiation with respect to x_1 produces

$$\frac{\partial}{\partial x_1} \log p(v|x_1) = \frac{k_1}{p(v|x_1)} \int_{-\infty}^{\infty} p(x_2)\, p(v|x_1, x_2) \int_0^T (v-s_1) \frac{\partial s_1}{\partial x_1}\, dt\, dx_2$$

$$- \frac{k_1}{p(v|x_1)} \int_{-\infty}^{\infty} p(x_2)\, p(v|x_1, x_2) \int_0^T s_2 \frac{\partial s_1}{\partial x_1}\, dt\, dx_2 \tag{A4}$$

The first expression in Eq.(A4) is easily simplified by integrating with respect to x_2. In the second expression we note that, if x_1 and x_2 are statistically independent, we have

$$\frac{p(x_2)\, p(v|x_1, x_2)}{p(v|x_1)} = p(x_2|v, x_1) \tag{A5}$$

With this Eq.(A4) is reduced to

$$\frac{\partial}{\partial x_1} \log p(v|x_1) = k_1 \int_0^T (v-s_1) \frac{\partial s_1}{\partial x_1}\, dt - k_1 \int_0^T \bar{s}_2 \frac{\partial s_1}{\partial x_1}\, dt \tag{A6}$$

where

$$\bar{s}_2(t) = \int_{-\infty}^{\infty} p(x_2|v, x_1) s_2\, dx_2 \tag{A7}$$

is recognized as the conditional mean and hence the minimum mean square estimate of $s_2(t)$.

Now following the second term in Eq. (6)

$$\frac{\partial}{\partial x_1} \log p(x_1) = \frac{\partial}{\partial x_1} \log \left\{ k_2 \exp \left[-\frac{1}{2} \left(x_1, R_{x_1}^{-1} x_1 \right) \right] \right\} = -\frac{1}{2} \frac{\partial}{\partial x_1} \left(x_1, R_{x_1}^{-1} x_1 \right) = -R_{x_1}^{-1} x_1 \tag{A8}$$

Again making use of Eq.(A2)to simplify Eq.(A8) and adding the result to Eq(A6) as per Eq. (6) we have after an inverse transformation

$$x_1(t) = k_1 \int_0^T R_{x_1}(t, u) \frac{\partial s_1}{\partial x_1} (v - s_1 - \bar{s}_2)\, du \tag{A9}$$

Solutions of Eq(A9) for $x_1(t)$ are the MAP estimates, we denote these by $\hat{x}_1(t)$. Further in Eq.(A9) it is noted that the integral on R. H. S. is a convolution integral in which the filter $R_{x_1}(t, u)$ is low-pass , whereas the term $s_1 \, \partial s_1 / \partial x_1$ involves double the carrier frequency terms and hence would integrate to zero. Eq.(A9) therefore simplifies to

$$\hat{x}_1(t) = k_1 \int_0^T R_{x_1}(t, u) \frac{\partial \hat{s}_1}{\partial x_1} \cdot (v - \bar{s}_2)\, du \tag{A10}$$

Eq. (A10) clearly shows a phase lock loop structure with $\bar{s}_2(t)$ as an external input as shown in Fig. 1.

Following all steps from Eq. (A1) through Eq. (A10) but estimating $x_2(t)$ instead of $x_1(t)$ we obtain

$$\hat{x}_2(t) = k_2 \int_0^T R_{x_2}(t, u) \frac{\partial \hat{s}_2}{\partial x_2} \cdot (v - \bar{s}_1)\, du \tag{A11}$$

This is a receiver identical to that in Fig. 1 except that $\bar{s}_2$ is replaced by $\bar{s}_1$ and $R_{x_1}(t, u)$ is replaced by $R_{x_2}(t, u)$.

Appendix B

Cross-Coupled PLL FM Demodulator Defining Equations

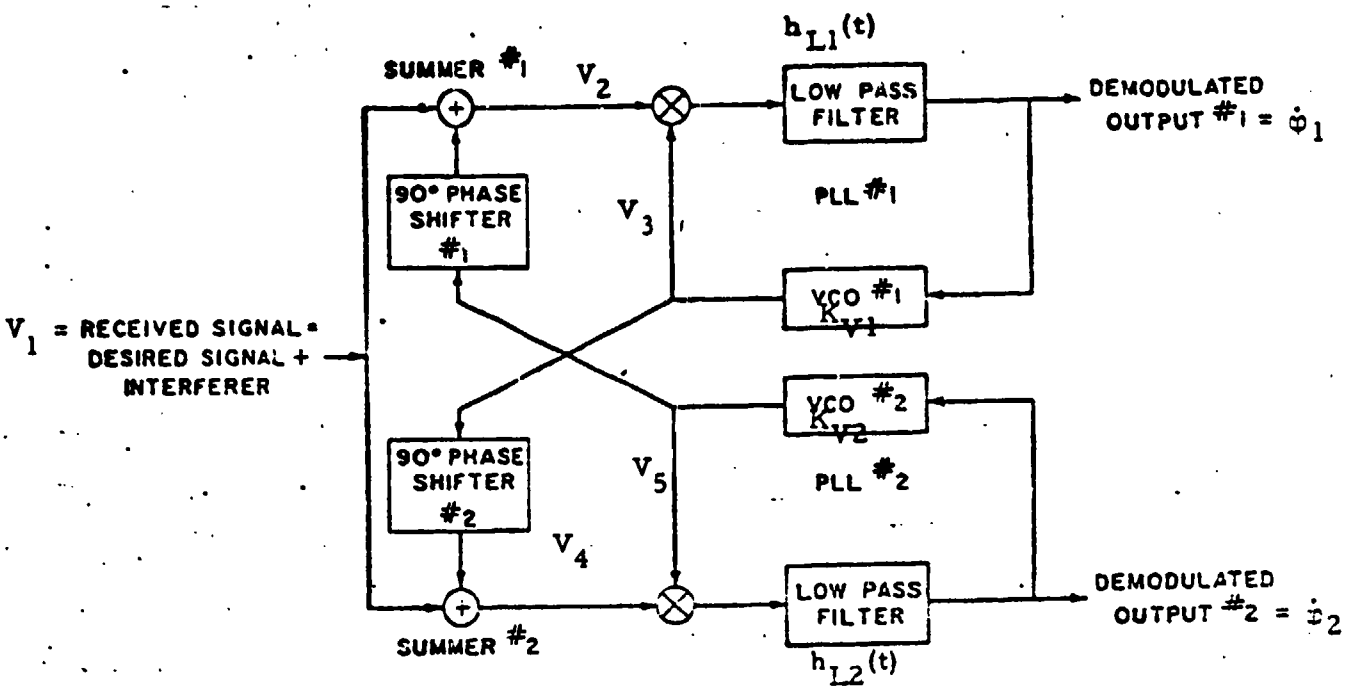

Theoretical Transient Acquisition Behavior

$$V_1(t) = \underbrace{A \sin[\omega_o t + \psi_1(t)]}_{\text{interferer}} + \eta \underbrace{A \sin[\omega_o t + \psi_2(t)]}_{\text{desired signal}} \qquad \text{(B-1)}$$

$$V_2 = A \sin[\omega_o t + \psi_1(t)] + \eta A \sin[\omega_o t + \psi_2(t)] - \eta A \sin[\omega_o t + K_{V2}\Phi_2]$$

$$\text{(B-2)}$$

$$V_3 = B \cos[\omega_o t + K_{V1}\Phi_1] \qquad \text{(B-3)}$$

$$\dot{\Phi}_1 = \left\{ \frac{AB}{2} \sin[\psi_1 - K_{V1}\Phi_1] + \frac{\eta AB}{2} \sin[\psi_2 - K_{V1}\Phi_1] - \frac{\eta AB}{2} \sin[K_{V2}\Phi_2 - K_{V1}\Phi_1] \right\} * h_{L1}(t) \qquad \text{(B-4)}$$

$$V_4 = A \sin[\omega_o t + \psi_1(t)] + \eta A \sin[\omega_o t + \psi_2(t)] - A \sin[\omega_o t + K_{V1}\varphi_1] \tag{B-5}$$

$$V_5 = B \cos[\omega_o t + K_{V2}\varphi_2] \tag{B-6}$$

$$\dot{\varphi}_2 = \left\{\frac{AB}{2} \sin[\psi_1 - K_{V2}\varphi_2] + \frac{\eta AB}{2} \sin[\psi_2 - K_{V2}\varphi_2] - \frac{AB}{2} \sin[K_{V1}\varphi_1 - K_{V2}\varphi_2]\right\} * h_{L2}(t) \tag{B-7}$$

Multiplying both sides of Eq. (4) by K_{V1} and Eq. (7) by K_{V2} and defining $K_{V1}\varphi_1 = \varphi_1^*$ and $K_{V2}\varphi_2 = \varphi_2^*$ yields

$$\dot{\varphi}_1^* = \left\{\frac{AB}{2} K_{V1} \sin[\psi_1 - \varphi_1^*] + \frac{\eta AB}{2} K_{V1} \sin[\psi_2 - \varphi_1^*] - \frac{\eta AB}{2} K_{V1} \sin[\varphi_2^* - \varphi_1^*]\right\} * h_{L1}(t) \tag{B-8}$$

$$\dot{\varphi}_2^* = \left\{\frac{AB}{2} K_{V2} \sin[\psi_1 - \varphi_2^*] + \frac{\eta AB}{2} K_{V2} \sin[\psi_2 - \varphi_2^*] - \frac{AB}{2} K_{V2} \sin[\varphi_1^* - \varphi_2^*]\right\} * h_{L2}(t) \tag{B-9}$$

dropping the * notation in Eq. (8) and Eq. (9) and normalizing by letting $\tau = \omega_N t$ yields,

$$\frac{d\varphi_1}{d\tau} = \frac{AB}{2} \frac{K_{V1}}{\omega_N} \left\{\sin(\psi_1 - \varphi_1) + \eta \sin(\psi_2 - \varphi_1) - \eta \sin(\varphi_2 - \varphi_1)\right\} * h_{L1}(\tau) \tag{B-10}$$

$$\frac{d\varphi_2}{d\tau} = \frac{AB}{2} \frac{K_{V2}}{\omega_N} \left\{\sin(\psi_1 - \varphi_2) + \eta \sin(\psi_2 - \varphi_2) - \sin(\varphi_1 - \varphi_2)\right\} * h_{L2}(\tau) \tag{B-11}$$

defining $\varphi_1' = \frac{d\varphi_1}{d\tau}$; $\varphi_2' = \frac{d\varphi_2}{d\tau}$; $\alpha_1 = \frac{\frac{AB}{2} K_{V1}}{\omega_N}$; $\alpha_2 = \frac{\frac{AB}{2} K_{V2}}{\omega_N} = \alpha_1 \cdot \frac{K_{V2}}{K_{V1}}$

produces

$$\varphi_1' = \alpha_1\{\sin(\psi_1-\varphi_1) + \eta\sin(\psi_2-\varphi_1) - \eta\sin(\varphi_2-\varphi_1)\}*h_{L1}(\tau) \qquad \text{(B-12)}$$

$$\varphi_2' = \alpha_2\{\sin(\psi_1-\varphi_2) + \eta\sin(\psi_2-\varphi_2) - \sin(\varphi_1-\varphi_2\}*h_{L2}(\tau) \qquad \text{(B-13)}$$

Equations (12) and (13) are the defining nonlinear coupled differential equations for the cross-coupled PLL FM demodulator with preadjusted summer constants. These equations were solved on the PDP 11/60 digital computer using Iteractive Graphics Language (IGL) for the case of first and second order loops.